Biocompatible 2D Materials via Liquid Phase Exfoliation

Yilin He, Andrés Felipe Andrade, Cécilia Ménard-Moyon, Alberto Bianco

Biocompatible 2D Materials via Liquid Phase Exfoliation

Yilin He, Andrés Felipe Andrade, Cécilia Ménard-Moyon, Alberto Bianco**

Y. He, A. F. Andrade, C. Ménard-Moyon, A. Bianco
CNRS, Immunology, Immunopathology and Therapeutic Chemistry, UPR 3572, University of Strasbourg, ISIS, 67000 Strasbourg, France
E-mail: a.bianco@ibmc-cnrs.unistra.fr, c.menard@ibmc-cnrs.unistra.fr

Keywords: Liquid phase exfoliation, two-dimensional materials, biocompatibility, bioapplications, bioactive molecules

Two-dimensional materials (2DMs), such as graphene, transition metal dichalcogenides (TMDs) and black phosphorus (BP), have been proposed for different types of bioapplications, owing to their unique physicochemical, electrical, optical and mechanical properties. Liquid phase exfoliation (LPE), as a one of the most effective up-scalable and size-controllable methods, is becoming the standard process to produce high quantity of various 2DM types as it can benefit of the use of green and biocompatible conditions. The resulting exfoliated layered materials have garnered significant attention because of their biocompatibility and their potential use in biomedicine as new multimodal therapeutics, antimicrobials and biosensors. In this review, we focused our attention on the production of LPE-assisted 2DMs in aqueous solutions with or without the aid of surfactants, bioactive or non-natural molecules. We further concluded with our insights into the possibilities of applications of such materials in the biological and biomedical fields.

1. Introduction

Graphene has emerged in 2004 as a two-dimensional (2D) carbon based-material, and, since then, it has attracted a lot of interests due to its unique mechanical, optical, electrical and thermal properties.[1-3] Thanks to these properties derived from its layered structure, graphene has been explored for many applications, such as energy storage, conductive coating, sensing and biomedicine.[4-8] The rapid development of researches on graphene has led to great interests on other 2D materials (2DMs) represented by hexagonal boron nitride (hBN), transition metal dichalcogenides (TMDs) and black phosphorus (BP), to cite the most exploited. With the expansion of the 2DM family, more and more 2DMs have been proposed for bioapplications ranging from cancer diagnosis and therapy to antibacterial and biosensing. For example, numerous studies have demonstrated that graphene with its large surface can be explored as a carrier to transport therapeutic drugs, peptides and genes.[9] The strong absorbance in the near-infrared (NIR) region allows graphene to be used in photothermal therapy (PTT).[10] Meanwhile, TMDs and BP have also potential applications in the biomedical field.[11-16] Interestingly, BP showed photo-induced generation of singlet oxygen making this material attractive for theranostics and antimicrobial use.[17,18] Compared with other 2DMs, hBN has instead not been much used as biomedical agent yet. Only few studies focused on its biocompatibility.[19]

To produce 2D layered materials, the bottom-up and top-down methods are two main approaches. Among all the bottom-up methods, chemical vapor deposition (CVD) is considered as a promising method for producing high quality graphene with large area. However, the quality of industrial production is still far from that of laboratory quality.[20] The top-down

method is based instead on the direct exfoliation of bulk materials to achieve thinner layers. Mechanical treatment, ion intercalation and liquid phase exfoliation (LPE) are three strategies for the top-down synthesis of 2DMs. Mechanical treatment provides a simple way to produce materials with high crystal quality. However, it faces the problem in achieving uniform samples with high yield. Ball milling is a technique that utilizes shear forces for exfoliation and can be employed for industrial production. Nonetheless, the intense grinding can induce a significant amount of defects on the surface of the 2DMs.[21] Among all these different exfoliation methods, LPE is widely regarded as the most effective way for producing various types of 2DMs with control over their size and thickness through adjustment of process parameters. Generally, LPE consists in sonication-assisted exfoliation and high-shear exfoliation. The bulk materials are first suspended in an appropriate solvent, either with or without the assistant of a surfactant, then subjected to sonication or high shear mixing. During the LPE process, the growth and collapse of the micrometer-sized bubbles or voids act on the bulk material and separate it into individual sheets.[22] The surfactant can additionally enhance the stability of the exfoliated sheets by intercalating between the layers to inhibit their tendency to re-aggregate. LPE is normally carried out in mild conditions, without high temperature or pressure. With high yield and tunable parameters, 2DMs obtained by LPE are suitable for various applications, especially in the biomedical field. However, the different LPE approaches and the chemical functionalization may affect the biocompatibility of the resulting materials. Therefore, it is fundamental to assess the adverse effects, such as toxicity, inflammation or immune responses, raised using 2DMs in guiding their potential clinical applications. Hence, the increased researches on 2DMs in biomedicine have led to parallel studies aimed at exploring their *in vitro* and *in vivo* toxicity.[23-25]

In this review, we will give a comprehensive summary of the studies on biocompatible LPE-assisted 2DMs and their applications in the biological and biomedical fields. The review is organized based on the different media used in LPE: i) surfactant-free LPE; in this part, we cover layered materials prepared directly in organic solvents or aqueous solutions, ii) non-natural molecule-assisted LPE; here, all dispersants used are non-natural molecules, such as small aromatic molecules and polymers, and iii) bioactive molecule-assisted LPE; in this section, we describe the bioactive molecules ranging from proteins, nucleotides and peptides to small bioactive molecules and biomacromolecules used to stabilize 2DMs during the exfoliation process. Table 1 provides a summary of the different works on biocompatibility and bioapplications using LPE-assisted 2DMs, which are discussed in this review. Overall, we aim

to provide an overview on LPE-assisted 2DM preparation, concluding with our perspectives on the opportunities and challenges for their biological and biomedical applications.

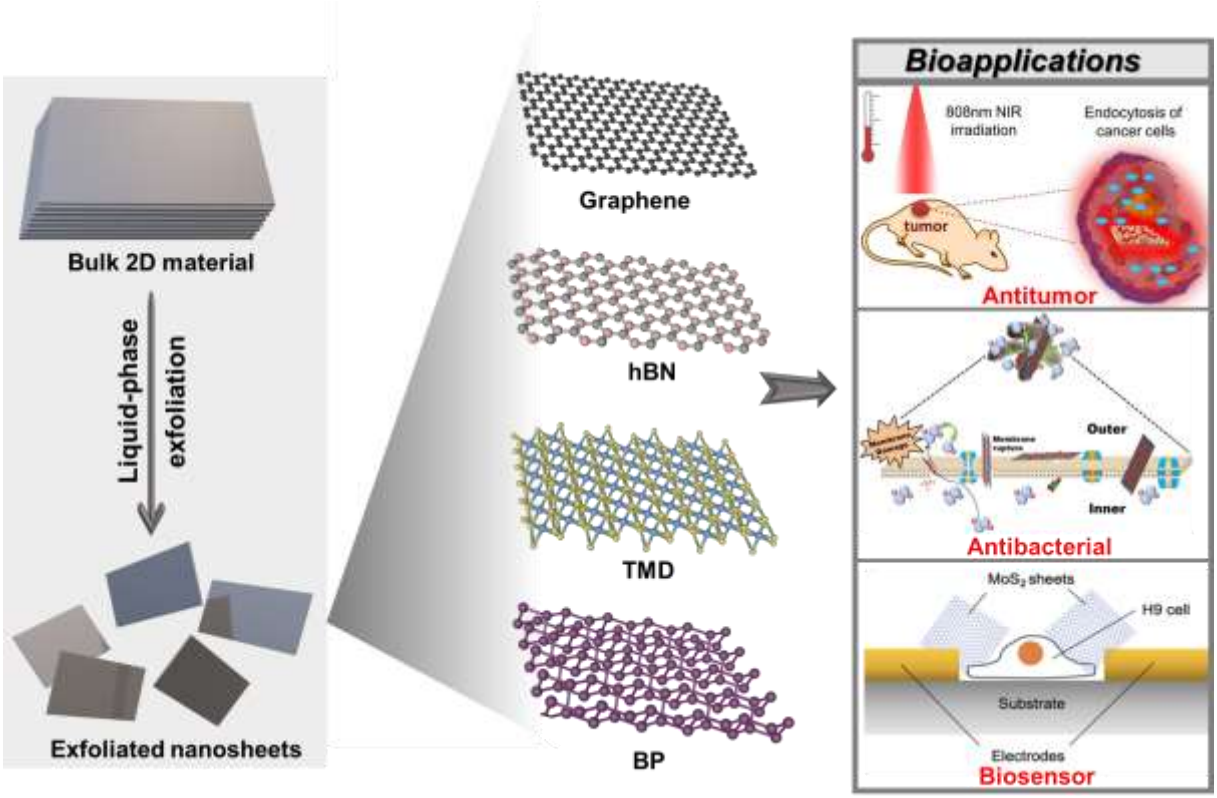

Figure 1. Preparation of 2DMs by LPE and their bioapplications. Reproduced with permission.[12] Copyright 2020, Wiley-VCH. Reproduced with permission.[13] Copyright 2018, American Chemical Society. Reproduced with permission.[25] Copyright 2014, American Chemical Society.

2. Surfactant-free exfoliation

2.1. Organic solvents

During LPE, solvents used to wet the bulk materials play a crucial role. By choosing the appropriate solvent, the potential energy stabilizing the adjacent layers can be efficiently reduced.[26] The physicochemical characteristics of a solvent, such as the surface tension, boiling points and solubility, can affect the efficiency of the exfoliation process.[27] *N*-methylpyrrolidone (NMP), dimethyl sulfoxide (DMSO), dimethylformamide (DMF), 2-butanone and some other organic solvents have been extensively evaluated for LPE of 2DMs.[23,28,29] It should be noted that it is a common practice to exchange the solvent after exfoliation to remove the organic solvent and obtain materials in aqueous phase. Among all the reported organic solvents, NMP has been found to be the most effective solvent to exfoliate

2DMs.[30,31] For instance, NMP-exfoliated BP nanosheets were applied for cancer therapy.[31] **Erreur ! Signet non défini.**In another study, BP was designed as a NIR-triggered nanoplatform for treating Alzheimer (**Figure 2a**).[32] After the removal of NMP by centrifugation, BP was covalently functionalized with a molecule having a high affinity for the amyloid-β. The capacity of layered BP to generate singlet oxygen under NIR irradiation was exploited to oxidize the amyloid-β peptide and inhibit its aggregation. The BP nanoplatform showed a high photo-oxygenation efficiency, a low cytotoxicity on PC12 rat pheochromocytoma tumor cells. Besides, BP nanosheets also possess a high NIR photothermal performance and are exploited as photothermal agent for PTT.[33] In order to enhance the stability and improve the dispersibility, polyethylene glycol (PEG) was simply coated on the layered BP by electrostatic adsorption in order to protect BP from hydrolysis and degradation and enhance the photothermal stability compared with non-coated BP. Moreover, BP-PEG showed a negligible cytotoxicity on L929 murine fibrosarcoma cells, 4T1 murine breast cancer cells and B16 murine melanoma cells. In combination with the immunoadjuvant imiquimod R837, BP-PEG exhibited a favorable photothermal-immunotherapy effect on melanoma *in vitro* and *in vivo*. A high immune response was induced, along with a higher release of cytokines (IL-6, IL-12 and TNF-α). Another photothermal agent, polypyrrole (PPy) in the form of nanoparticles, was complexed to BP nanosheets to improve their photothermal capacity.[34] Exfoliated BP and BP-PPy both showed a negligible toxicity on 4T1 cells. *In vitro* and *in vivo* experiments demonstrated a satisfactory anti-tumor capacity. Apart from PTT, BP nanosheets exfoliated by NMP have been designed as a delivery system for small interfering RNA (siRNA) delivery.[35] Positively charged polyethylene imine (PEI) was coated on BP nanosheets, followed by the loading of the apoptosis inhibitor siRNA survivin to silence the expression of survivin protein. The stability in biological media and bioavailability of siRNA was improved, as the BP-PEI protects siRNA from enzymatic degradation, thus enhancing the efficiency of the gene transfection. BP-PEI exhibited a low toxicity toward MCF-7 breast cancer cells. BP-PEG-siRNA was effective in inhibiting the tumor growth, which was enhanced under NIR irradiation.

MoS_2 and WS_2 have been also exfoliated by NMP, and the resulting materials have been exploited as therapeutic nanomedicines for tumor therapy and imaging. MoS_2 can be used as a co-catalyst for the Fenton reaction. For instance, exfoliated MoS_2 was conjugated to Fe(III) through gallic acid (GA) to enhance chemodynamic therapy (CDT) (**Figure 2b**).[36] Both MoS_2 and MoS_2@GA showed good biocompatibility on HepG2 human liver cancer cells, but the cell viability decreased when treated with MoS_2@GA-Fe. In the tumor, which is slightly acidic, a large amount of hydroxyl radicals was generated through Fe(III)-based Fenton reaction.

Moreover, the photoacoustic imaging (PAI) feature of MoS_2 and the magnetic resonance imaging (MRI) thanks to iron were used to guide CDT *in vivo*. Alternatively, NMP-exfoliated WS_2 was explored as a theranostic agent for PTT and X-ray computed tomography (CT) imaging (**Figure 2c**).[37] Bovine serum albumin (BSA) protein was coated onto the surface of WS_2 to impart a good biocompatibility. *In vivo* experiments were performed on the zebrafish embryo model, indicating that the hatching rate and development were delayed, but there was no significant effect on tail morphology and fry activity of the zebrafish. WS_2@BSA also effectively inhibited the growth of HeLa human cervical cancer cells by PTT.

Apart from NMP, DMF and DMSO can be also utilized to exfoliate bulk materials.[38,39] The dimension of 2DMs has effects on their cytotoxicity. Three kinds of BP with different sizes (average size of large BP (L-BP): 394 nm, medium BP (M-BP): 118 nm and small BP (S-BP): 4.5 nm) were prepared by exfoliation in DMSO.[39] The three BP nanosheets showed nearly no inhibition on the cell growth of LO2 human fetal hepatocyte cells. Noticeably, all types of BP sheets had a strong photothermal effect on MCF-7 cancer cells, while L-BP exhibited the best photothermal performance to induce cancer cell death. In another work, 2-butanone was used to exfoliate TMDs and hBN.[23] Exfoliated MoS_2 did not inhibit the growth of mixed glial cells, while the cell viability decreased drastically after the treatment with hBN. In the presence of human myeloperoxidase and hydrogen peroxide, both MoS_2 and hBN were degraded via reactive intermediates generated during the enzymatic reaction and the formation of hypochlorite ions. The time to achieve full degradation of 2H-MoS_2 was 30 h, while 1T-MoS_2 had a faster degradation rate in the presence of hydrogen peroxide than treated with the combination of human myeloperoxidase and hydrogen peroxide.[40] The faster rate of 1T-MoS_2 may be derived from the higher thermodynamic stability of 2H-MoS_2. Alternatively, hBN was degraded much more slowly than MoS_2. The same degradation performance of hBN has been reported in another article using sodium cholate-exfoliated hBN.[41] The exfoliated hBN exhibited partial degradation by human myeloperoxidase.

Other organic solvents, including isopropanol (IPA), have been used for LPE of 2DMs.[42-44] As an example, BP nanosheets prepared by exfoliation in IPA were decorated with polyoxometalates (POMs) for enhanced PTT (**Figure 2d**).[43] The exfoliated BP was dispersed in water by a solvent exchange process, followed by the conjugation of a NH_2-PEG-SH and POMs. By exploiting the acid-aggregation behavior of POMs, the photothermal efficiency of POM@BP was enhanced. Because the scattering cross-section increases with the particle size, the interaction between neighboring functionalized BP nanosheets was significantly enhanced, leading to a greater conversion of light energy into heat. The BP nanosheets and POM@BP not

only showed no obvious effect on the cell viability of Huh7 hepatoma cells, HepG2 cells and HeLa cells, but also had no significant toxicity on the kidney and liver of mice, demonstrating a highly biocompatibility. POM@BP efficiently inhibited tumor growth. Additionally, BP nanosheets exfoliated in IPA were also applied for the enrichment and elimination of circulating tumor cell (CTC).[44] PEG was conjugated onto the BP nanosheets. The biocompatibility assessed by hematological and histological analyses after *in vivo* administration was high. An intravenous indwelling catheter was filled with the PEG-BP and modified with an anti-EpCAM (epithelial cell adhesion molecule) antibody in the exterior surface. The captured CTCs were collected for further analysis or treated *in situ* by PTT. The catheter was able to capture HepG2 and HeLa cells *in vivo* using a rabbit model. Besides, *N*,*N*′-dimethylpropyleneurea (DMPU), a more harmless and environmental friendly solvent compared with NMP, has also been used for highly efficient exfoliation of BP.[45] The exfoliated BP can reach a high concentration of 1.11 mg/mL with a yield of 16%. The layered BP exhibited a good stability and high resistance against oxidation, probably owing to the protection of DMPU molecules. The DMPU-exfoliated BP nanosheets were able to kill *E. coli* and *S. aureus* up to 99.2%, which was much higher compared to bulk BP, graphene and IPA-exfoliated 2D MoS_2, showing a thickness-dependent antibacterial property. In contrast, BP had a negligible toxicity on HeLa cells even at the concentration of 1.28 mg/mL.

Finally, cyclopentanone is another alternative solvent for the exfoliation of graphene and MoS_2.[46,47] Cyclopentanone-exfoliated MoS_2 was not toxic to U2OS epithelial morphology cells and 1BR primary fibroblasts.[48] Raman mapping of the U2OS cells evidenced that most of the MoS_2 nanosheets accumulated near the nuclear region, while some materials were located in the cytoplasm. The decomposition of the MoS_2 nanosheets started from the edges, as the thickness of MoS_2 remained the same while the lateral size became shorter.

All above studies demonstrated that organic solvents are powerful for LPE to reach high efficiency, which could be expanded to large-scale production. This strategy requires simple operation, guarantees high repeatability and good quality of the exfoliated 2DMs. Nevertheless, after the exfoliation process, there can still be a risk that traces of organic solvents remain trapped on the exfoliated nanosheets. The residual organic solvents may potentially induce health and environmental risks. To mitigate this issue, a thorough purification or the use of non-toxic reagents can overcome this problem.

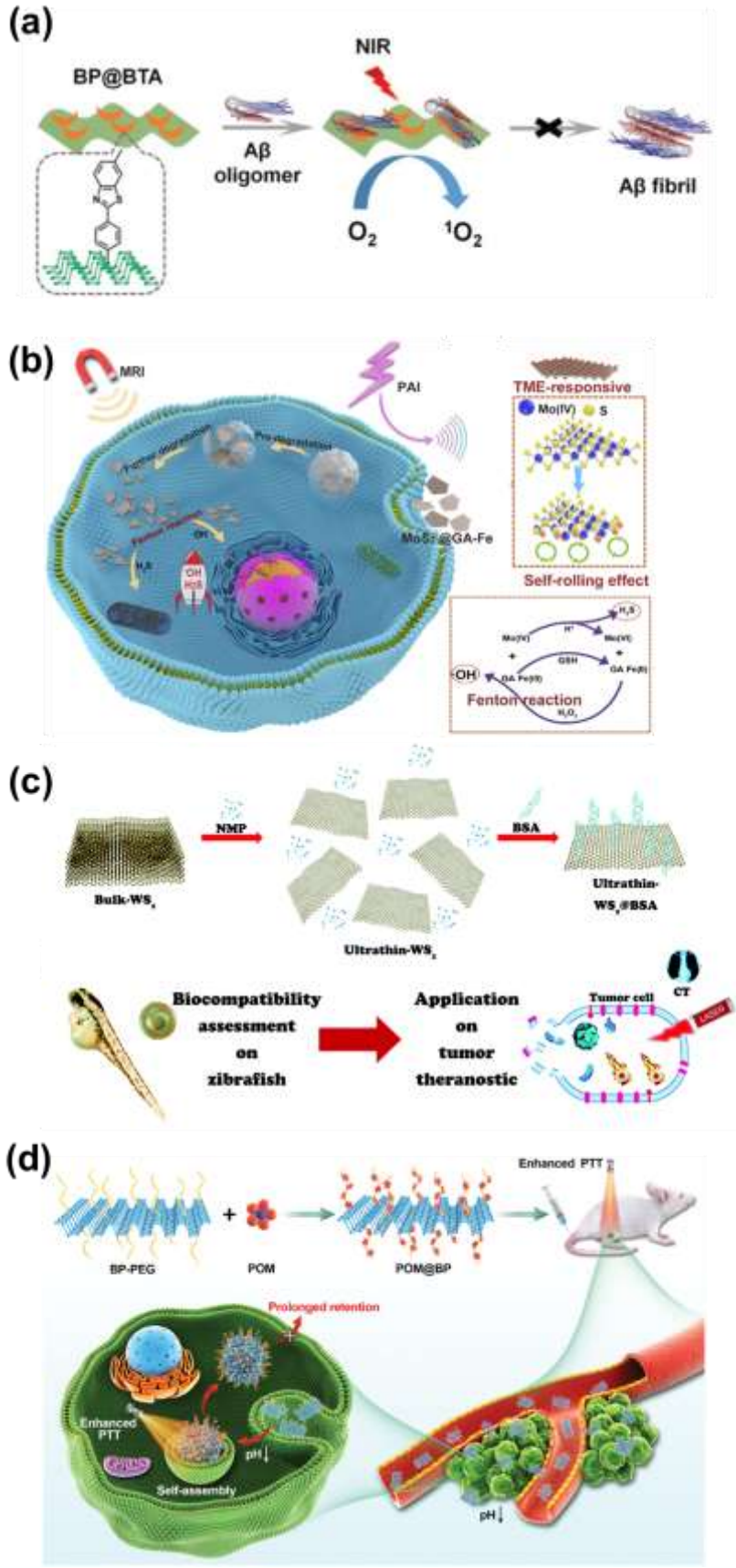

Figure 2. Exfoliation of 2DMs in organic solvents and their applications in the biomedical field. (a) NMP-exfoliated BP nanosheets conjugated with one of the thioflavin-T derivatives, 4-(6-

methyl-1,3-benzothiazol-2-yl) phenylamine (BTA) for NIR-triggered production of singlet oxygen to inhibit amyloid-β aggregation and treat Alzheimer's disease. Reproduced with permission.[32] Copyright 2019, Wiley-VCH. (b) GA-modified MoS_2 loaded with Fe(III) for MRI/PAI-guided CDT. Reproduced with permission.[36] Copyright 2021, Elsevier. (c) Biocompatibility and tumor theranostics of NMP-exfoliated WS_2 coated with BSA in a zebrafish embryo model. Reproduced with permission.[37] Copyright 2021, Royal Society of Chemistry. (d) Preparation of POM-loaded PEG-BP nanosheets for enhanced PTT through acid-induced aggregation. Reproduced with permission.[43]. Copyright 2020, Wiley-VCH.

2.2. Aqueous phase

Although organic solvents have been substantially used to exfoliate 2DMs, they strongly interact with the surface, may affect further modification and induce some toxicity in case residual solvent molecules remain, thus limiting their biological applications.[49] The exfoliation in pure water has attracted many interests, as water is non-toxic and eco-friendly, and the process is cost-effective. However, this method is endowed of a big challenge, as most 2DMs have a low dispersibility in water restricting the efficiency of exfoliation in an aqueous phase.[50] However, in the past few years, several approaches have been reported showing the possibility of exfoliation in pure water with biosafety for bioapplications, such as biosensing and cancer diagnosis.[13,51,52] Bulk BP can be easily exfoliated in ice water for 8-12 hours to produce exfoliated nanosheets, with nitrogen bubbling as the initial step to avoid oxidation.[53-56] In contrast, the exfoliation in pure water of other materials, such as MoS_2, WS_2 and hBN, requires a longer time (60 hours).[57] Unfortunately, graphene can hardly be exfoliated directly in water due to its hydrophobic surface. Therefore, pure water-exfoliation is considered as a worthy option to produce nanosheets, especially for BP, in bioapplications. For example, water-exfoliated BP was shown to be an efficient photosensitizer through the generation of singlet oxygen with a high quantum yield.[53] The BP sheets showed a good biocompatibility on MDA-MB-231 breast cancer cells in the dark, while cell death was observed under 660-nm irradiation. *In vivo* the BP nanosheets effectively hindered the growth of tumor and reduced the tumor volume under light irradiation by photodynamic therapy (PDT). In another study, layered BP displayed a size-dependent cytotoxicity.[54] BP with different size and thickness, prepared by aqueous phase exfoliation, were separated by different centrifugation speeds. Interestingly, the largest BP (lateral size of 884 nm) exhibited the highest cytotoxicity on NIH3T3 embryonic mouse fibroblast cells, human colonic epithelial cells (HCoEpiC), and 293T human embryonic kidney cells, which was associated to the generation of reactive oxygen species (ROS) and

physical damage of the cell membrane. In contrast, the smaller BP was able to promote cell proliferation even at low concentration, likely due to the release of phosphate ions arising from the degradation of BP. Water-exfoliated BP nanosheets have been also employed as theranostic drug delivery platforms (**Figure 3a**).[55] In this study, BP with an average height of 1-2 nm was prepared in water with bubbled-argon to minimize the oxidation during the exfoliation. A PEG-amine derivative was then adsorbed on the BP sheets via electrostatic interactions to improve the stability and biocompatibility. As shown in **Figure 3a**, doxorubicin (DOX) and cyanine 7 (Cy7) were loaded onto the PEGylated BP for drug delivery and *in vivo* NIR fluorescence imaging, respectively, while a folic acid (FA)-modified PEG (FA-PEG-NH_2) and a fluorescein isothiocyanate (FITC)-conjugated PEG (FITC-PEG-NH_2) were adsorbed onto PB for targeting and *in vitro* fluorescence imaging, respectively. FA has the capacity to bind to folate receptors, which are overexpressed on many cancer cells. The BP-PEG-FA showed excellent PTT performance on HeLa cells. The BP-PEG-FA/DOX were internalized into the cancer cells via endocytosis and micropinocytosis, inducing a high intracellular toxicity. Biodistribution studies using the Cy7-loaded BP-PEG showed that after 24 h BP was accumulated at the tumor site due to the enhanced permeability retention (EPR) effect and the targeting capacity of FA. BP-PEG-FA/DOX exhibited favorable therapeutic effects *in vivo* without side effects or toxicity. BP nanosheets can also be combined with other nanomaterials for bioapplications. In one study, gold and Fe_3O_4 nanoparticles were complexed onto water-exfoliated BP through electrostatic interactions to form BP@Au@Fe_3O_4 and were exploited for combined PDT and PTT in anticancer therapy.[56] The BP@Au@Fe_3O_4 exhibited a low cytotoxicity on L929 cells even at 1 mg/mL. The *in vivo* biocompatibility was evaluated using a serum biochemistry assay, indicating a low hepatic toxicity. Besides, thanks to the Fe_3O_4 nanoparticles, BP@Au@Fe_3O_4 was used *in vivo* as a T_2 contrast agent for MRI.

The exfoliation in water at high temperature can be used to improve the yield and colloidal stability of 2D nanosheets. Layered hBN, MoS_2, WS_2 and $MoSe_2$, have been successfully exfoliated in pure water with the control of the temperature (30 °C and 60°C).[57] Unfortunately, graphite could not be exfoliated directly in water because of its hydrophobic nature, but it was exfoliated under weakly basic condition (pH=11). The OH^- ions on the surface endowed graphite with a good colloidal aqueous stability.[58] Besides, water-exfoliated MoS_2 nanosheets were exploited as nanoplatforms for cancer cell detection after functionalization with an antibody for recognition.[59] Thanks to the high affinity of the dithiolane moiety of lipoic acid for the sulfur vacancies of MoS_2, lipoic acid-sulfobetaine and lipoic acid-PEG-biotin were covalently bound to the MoS_2 sheets. The sulfobetaine group was used to prevent non-specific

protein adsorption onto the MoS_2. A M75 antibody, having the capacity to specifically bind to carbonic anhydrase IX overexpressed on cancer cells, was conjugated through a biotin–avidin–biotin bridge. The water-exfoliated MoS_2 with or without functionalization showed no cytotoxicity on JIMT-1 cancer cells and noncancerous MRC5 cells. The antibody-loaded MoS_2 platform was internalized more into JIMT-1 cancer cells than noncancerous MRC5 cells. In another study, the impact of water-exfoliated MoS_2 on soil bacteria *B. cereus* and *P. aeruginosa* was evaluated.[60] The toxicity of the MoS_2 sheets on the bacteria was higher than the bulk MoS_2, but lower than conventional antimicrobial agents. Both bulk and exfoliated MoS_2 impeded the growth of the soil bacteria. In particular, wrinkles and rhytids on the bacterial wall were observed by scanning electron microscopy when the bacteria were incubated with the exfoliated MoS_2. In contrast, there was no significant sign of morphological damages in the presence of the bulk MoS_2, probably because the material with the smaller lateral size and thinner sheets can better conform to the curvature of bacteria. Besides, the treatment with the exfoliated MoS_2 induced oxidative stress leading to an efficient antibacterial effect. Apart from the antibacterial properties, the cytocompatibility of the exfoliated MoS_2 sheets were also studied.[61] The results showed that the MoS_2 nanosheets were able to induce cell death on tumor cells (U937 and MCF-7), but the effect on normal cells (HaCaT) was negligible although some mechanical damages were found in all three cell lines. Therefore, the MoS_2 nanosheets could be exploited for anticancer therapy. In the same study, owing to its sharp edges MoS_2 can serve as a nano-knife to cut the *Salmonella* bacterial membrane. In another article, the biodegradability of water-exfoliated MoS_2 and their biocompatibility *in vitro* and *in vivo* were assessed.[62] MoS_2 was first dispersed in H_2SO_4 and heated at 90°C, followed by washing several times with deionized water. The H_2SO_4-treated MoS_2 was then exfoliated in an aqueous phase, followed by the decoration with polyvinylpyrrolidone (PVP) to improve the water dispersibility. The MoS_2-PVP induced no toxicity on human umbilical vein endothelial cells (HUVECs) and human hepatoma cell line (SMMC-7721) at a concentration below 200 μg/mL, whereas a high toxicity was observed at 400 μg/mL. By transmission electron microscopy and synchrotron radiation transmission X-ray microscopy, MoS_2-PVP was found to be endocytosed, accumulate in the lysosomes and finally be excreted by exocytosis. Compared with MoS_2, MoS_2-PVP exhibited a higher biodegradability in physiological concentrations of H_2O_2 and in the presence of human myeloperoxidase. Additionally, the biodistribution of MoS_2-PVP was investigated by inductively-coupled plasma mass spectrometry and fluorescence imaging. MoS_2-PVP was gradually degraded and cleared in the liver and spleen after intravenous injection into mice. The

clearance and biosafety of MoS_2-PVP was confirmed by hematological and histological examinations, providing opportunities for bioapplications.

Beside exfoliation in pure water, a mixed-solvent method was also explored to produce highly stable exfoliated 2DMs, such as MoS_2, WS_2 and hBN.[63] An interesting study reported the preparation of MoS_2 nanoplates, by making use of the mixed-solvent strategy, loaded with a chlorin e6-aptamer for intracellular adenosine triphosphate (ATP) detection and PDT.[64] The fluorescence of chlorine e6 was quenched because of interactions with MoS_2. Owing to the high affinity of the aptamer for ATP, chlorine e6 was released from the MoS_2 nanoplates after internalization into cells and binding to ATP, resulting in the recovery of the fluorescence of chlorine e6. The released chlorine e6 was thus able to monitor the ATP level in living cells through *in situ* "off-on" fluorescence and could produce $^1O_2$ under irradiation at 660 nm to induce cell death. In another study, MoS_2 conjugated with an anti-CD33 antibody was designed for targeting and monitoring the cellular uptake of acute myeloid leukemia cells (**Figure 3b**).[65] MoS_2 was exfoliated in 45% (v/v) ethanol/water mixture and functionalized with lipoic acid-PEG-biotin. Alexa Fluor 488-labeled avidin was bound on the functionalized MoS_2 through the formation of a biotin-avidin complex, followed by the conjugation of the biotinylated anti-CD33 antibody. The cell viability on SKM-1 (established acute myeloid leukemia cell line) was around 70% at the concentration of 5 μg/mL. MoS_2 accumulated in the cells through the recognition between the anti-CD33 antibody and the specific CD33 receptors on the SKM-1 cells. The antibody-functionalized MoS_2 proved an efficient approach for future diagnosis and treatment of acute myeloid leukemia.

In another study, an $Ag_2S@WS_2$ complex was used as an antibacterial agent (**Figure 3c**).[66] The WS_2 nanosheets were sonicated in 45% (v/v) ethanol/water solution to prepare individual nanosheets, followed by *in situ* growth of Ag_2S nanoparticles on the WS_2 surface. Thanks to the tight contact between WS_2 and Ag_2S, under 808-nm laser irradiation a transfer of photo-activated electrons occurred from Ag_2S to WS_2, leading to the production of ROS. In addition, as a result of the increase of NIR light absorbance due to WS_2, $Ag_2S@WS_2$ displayed a better photothermal performance than Ag_2S alone. The antibacterial efficiency of $Ag_2S@WS_2$ was found to be 99.93% and 99.84% on *S. aureus* and *E. coli*, respectively, resulting from the combination of the photocatalytic and the photothermal effect. Apart from the remarkable antibacterial properties, the presence of the Ag_2S nanoparticles improved the cytocompatibility of WS_2 on MC3T3-E1 cells. Not only a mixture of water and ethanol can be used for LPE, but also a mixture of DMSO and deoxygenated water. For example, BP exfoliated in DMSO/deoxygenated water (1000:1) showed a great potential for osteosarcoma treatment.[67]

The layered BP triggered the production of ROS in osteosarcoma cells under NIR light irradiation and exhibited antiproliferative and apoptotic effects. In contrast, only a low toxicity on healthy bone-derived human adult osteoblasts (HOb) cells was observed. Besides, the exfoliated BP also showed anti-inflammation activity on coculture models of human primary osteogenic sarcoma cells (SAOS-2) and HOb cells. The production of proinflammatory mediators was reduced, while it was increased for the anti-inflammatory cytokine IL-10.

Overall, the exfoliation in pure water is considered the cheapest "green" solution to produce 2DMs for biomedical applications. Although water as an exfoliation solvent is not very effective to get high exfoliation yields, the absence of organic solvent molecules potentially adsorbed onto the nanosheets guarantees a high biocompatibility and 2DMs produced by this surfactant-free approach are more conducive to subsequent chemical surface modification.

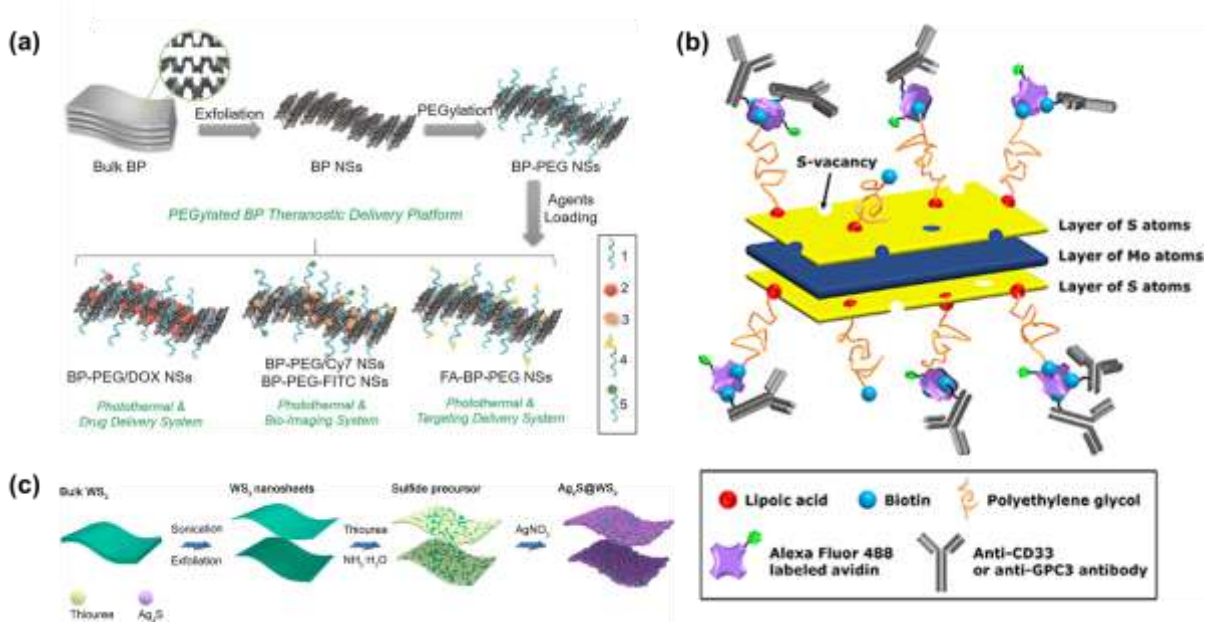

Figure 3. Strategies applied to exfoliate BP and TMDs in aqueous phase for bioapplications. (a) Water-exfoliated BP functionalized with different agents for cancer diagnosis and therapy. 1: PEG-NH_2, 2: DOX, 3: Cy7-NH_2, 4: FA-PEG-NH_2, 5: FITC-PEG-NH_2. Reproduced with permission.[55] Copyright 2017, Wiley-VCH. (b) Functionalized MoS_2 for targeting and monitoring the cellular uptake of acute myeloid leukemia cells. Reproduced with permission.[65] Copyright 2021, IOP Science. (c) Exfoliation of WS_2 and functionalization with Ag_2S nanoparticles through *in situ* growth. Reproduced with permission.[66] Copyright 2019, American Chemical Society.

3. Non-natural molecules

3.1. Small aromatic molecules

Many exfoliating agents have been used for LPE to increase the exfoliation yield and improve the stability of the resulting suspensions. They serve as stabilizers by adsorbing onto the layered materials, thus preventing their aggregation. In particular, small aromatic molecules, such as pyrene derivatives, have been used for the effective exfoliation of 2DMs. Through non-covalent interactions, the aromatic core of the pyrene can intercalate between the layers and adsorb on the surface, while the functional groups enhance the solvation and stability of the suspensions.[68] For example, graphene, MoS_2, WS_2 and hBN have been successfully exfoliated by 1-pyrenesulfonic acid (PS1), leading to the formation of water-based, ink-jet-printable inks.[69] The printing solvent, containing propylene glycol, water, Triton x-100 and Xanthan gum, were employed to disperse the exfoliated materials to prepare printing ink. The potential risk of the 2DM-based inks on living organisms was evaluated on human lung cancer cells A549 and skin HaCaT cells, showing no significant cytotoxic responses, demonstrating their potential use for consumer products, such as smart packaging applications and identification tags. The study of the biocompatibility of PS1-exfoliated MoS_2 and WS_2 was also performed on human macrophages in which no inhibition on the cell growth and no pro-inflammatory response were induced. Besides using PS1 as exfoliating reagent, other pyrene derivatives have also been investigated to improve the yield and suspension stability. For instance, a bis-pyrene derivative and a series of cationic amphiphilic pyrenes were used for the exfoliation of graphene (**Figure 4a** and **b**).[70,71] Human non-tumorigenic lung epithelial BEAS-2B and HeLa cells treated with graphene exfoliated with a pyrene bearing a trimethylammonium group presented no obvious morphological damages or decrease of cell. Besides, graphene exfoliated by cationic amphiphilic pyrenes showed a higher internalization by BEAS-2B and HeLa cells than the negatively charged PS1-exfoliated graphene, according to the higher affinity between cationic molecules and the negatively charged proteoglycans on the cell membrane. Liquid cascade centrifugation was used to prepare graphene sheets with different sizes exploiting bis-pyrene (BPS), a pyrene derivative that consist of two pyrene cores linked by a pyrrolidone central group.[72] It was noticed that the initial amount of BPS affected the toxicity of the graphene nanosheets. The lower amount of BPS led to the best cytocompatibility on BEAS-2B cells. From the *in vitro* experiments, the concentration of exfoliated graphene at 0.4 mg/mL was considered as a critical concentration, as the stability and biocompatibility decreased above this concentration. Besides, the cytotoxicity was also related to the size of graphene, as the smaller size exhibited a higher toxicity. Overall, pyrene derivatives have been explored for the effective exfoliation of 2DMs, especially graphene, to obtain high quality and high concentration suspensions. However, the potential toxicity of pyrene derivatives might be a limiting factor.

3.2. Surfactants

In addition to aromatic molecules, several surfactants have been explored for the exfoliation of 2DMs. Compared with aromatic molecules, some surfactants can better enhance the dispersibility and biocompatibility of 2DM suspensions. For example, cationic cetyltrimethylammonium bromide (CTAB) is a positively charged surfactant used to exfoliate graphene through hydrophobic interactions.[73] Aiming to study the antimicrobial behavior of the material, the CTAB-exfoliated graphene suspension was filtered to form a film. Two samples of graphene with different surface topographic properties, a smooth graphene (named GN-S, corresponding to the surface facing the filter) and a rough one (named GN-R, the top surface of the film), were collected. Both *S. aureus* and *P. aeruginosa* were able to attach to the cationic graphene nanosheets, but the bacterial cells adhered more to the smooth graphene. When bound to the surface of GN-S and GN-R, the morphology of the two bacteria changed, leading to cell death. The cell viability of *S. aureus* was lower on GN-R compared to GN-S. Through simulation and fluorescence experiments, it was found that the antibacterial behavior of graphene was mostly dependent on its lipophilicity. The nanosheets can cut the bacterial cell membrane and induce the formation of pores, further changing the osmotic pressure and causing bacterial death. Apart from CTAB, Pluronic copolymers, such as F108 and L64, were also used to exfoliate graphene and other 2DMs thanks to their hydrophobic interactions able to improve the dispersibility and biocompatibility of these materials. Indeed, compared with CTAB-exfoliated graphene, Pluronic-exfoliated graphene showed much lower cytotoxicity.[74,75] No cell death was observed at the concentration of 0.65 μg/mL, whereas nearly all cells were dead when the concentration reached 34 μg/mL. While Pluronic-exfoliated graphene exhibited reduced cytotoxicity in comparison to CTAB-exfoliated graphene, it still exhibited a moderate toxic effect. Compared with PS1-exfoliated graphene that maintained a cell survival rate of 80-90% at a concentration of 100 μg/mL, the toxicity of Pluronic-exfoliated graphene was significant.[72] Indeed, the surfactant degraded during the exfoliation process and it was considered as the dominant factor that induced cell death. Nevertheless, under NIR light irradiation the Pluronic-exfoliated graphene induced the death of NG108-15 neuronal cells at the concentration of 17 μg/mL. The Pluronic surfactant F127 was also employed to exfoliate hBN by bath or tip sonication, the latter allowing a more efficient production of few-layered nanosheets with high yield (**Figure. 4c**).[76] Thanks to the coating of Pluronic F127, the exfoliated hBN possessed an improved dispersibility and cytocompatibility on HeLa cells even when the concentration reached 200 μg/mL. Overall, graphene and other 2DMs have been

effectively exfoliated by different surfactants. Nevertheless, for bioapplications, the presence of surfactants in the aforementioned studies might be a concern as a low biocompatibility was identified in some cases. To overcome this issue, the toxicity mechanisms need to be carefully studied.

3.3. Polymers

Polymers with a good biocompatibility were found to be efficient exfoliating agents to obtain water-soluble and functional nanosheets.[77,78] Polyvinylpyrrolidone (PVP), a nonionic and nontoxic polymer, has been widely used as an exfoliating agent.[79] The hydrophilic nature of PVP, along with the presence of substituents on the nitrogen atom of the pyrrolidone ring, making the structure similar to NMP, can contribute to enhancing the colloidal stability of aqueous nanosheet suspensions. Meanwhile, PVP-exfoliated nanosheets display a good biocompatibility and are suitable for bioapplications. For instance, PVP coated-graphene induced the death of U251 human glioma cells by PTT and the photothermal performance was higher compared to carbon nanotubes.[80] Upon NIR light irradiation, graphene caused oxidative stress and mitochondrial depolarization, leading to apoptotic/necrotic cells. Alternatively, PVP was used to exfoliate MoS_2.[81] Bulk MoS_2 was sonicated in the presence of PVP in a water/ethanol mixture, then added into supercritical CO_2 to create an emulsion microenvironment for further exfoliation. Thanks to the quantum size effect, the exfoliated MoS_2 with a size less than 120 nm displayed photoluminescence properties, making it suitable as a fluorescent label for cell imaging. The toxicity was tested on human U251 cells and the PVP-stabilized MoS_2 nanosheets showed a good biocompatibility. Other polymers that share similar physicochemical properties with PVP were also considered as exfoliating agents. Four different types of vinylimidazole-based polymers were synthesized to exfoliate graphene in aqueous phase, achieving stable suspensions with the highest concentration of 1.12 mg/mL.[82] The vinylimidazole-based polymers containing a pyrene moiety exhibited a better exfoliation efficiency thanks to a higher adsorption capacity on graphene due to strong π-stacking interaction. The cell viability of the resulting graphene sheets on L-929 mouse fibroblast cells was low and comparable to the PVP-graphene. In another study, hyperbranched polyglycerol modified with aromatic moieties was used for the exfoliation of graphene.[83] The polyglycerol on the graphene nanosheets prevented the adsorption of serum proteins. The exfoliated graphene was effectively internalized into the cytoplasm of MCF-7 cells showing a low cytotoxicity, whereas inhibition of the cells was observed when exposed to NIR light irradiation due to the photothermal effect of graphene. In addition to the polymers mentioned above,

poly(acrylic acid) (PAA) was used to exfoliate graphene in aqueous medium. Then, PAA-graphene formed a hydrogel in the presence of acrylic acid, the cross-linker *N*,*N*-methylenebisacrylamide and ammonium persulfate.[84] The hydrogel was non-toxic on MG-63 human osteosarcoma cells and displayed cell adhesion properties. The deprotonation of the carboxylic acids of PAA at basic pH induced the swelling of the hydrogel, resulting in the release of diltiazem hydrochloride. In general, water-soluble polymers with high biocompatibility are suitable exfoliating agents. The work mentioned above demonstrated effective exfoliation, leading to the utilization of the resulting 2D sheets for biological applications. Nevertheless, exploring alternative biocompatible polymers is still relevant for LPE of 2DMs.

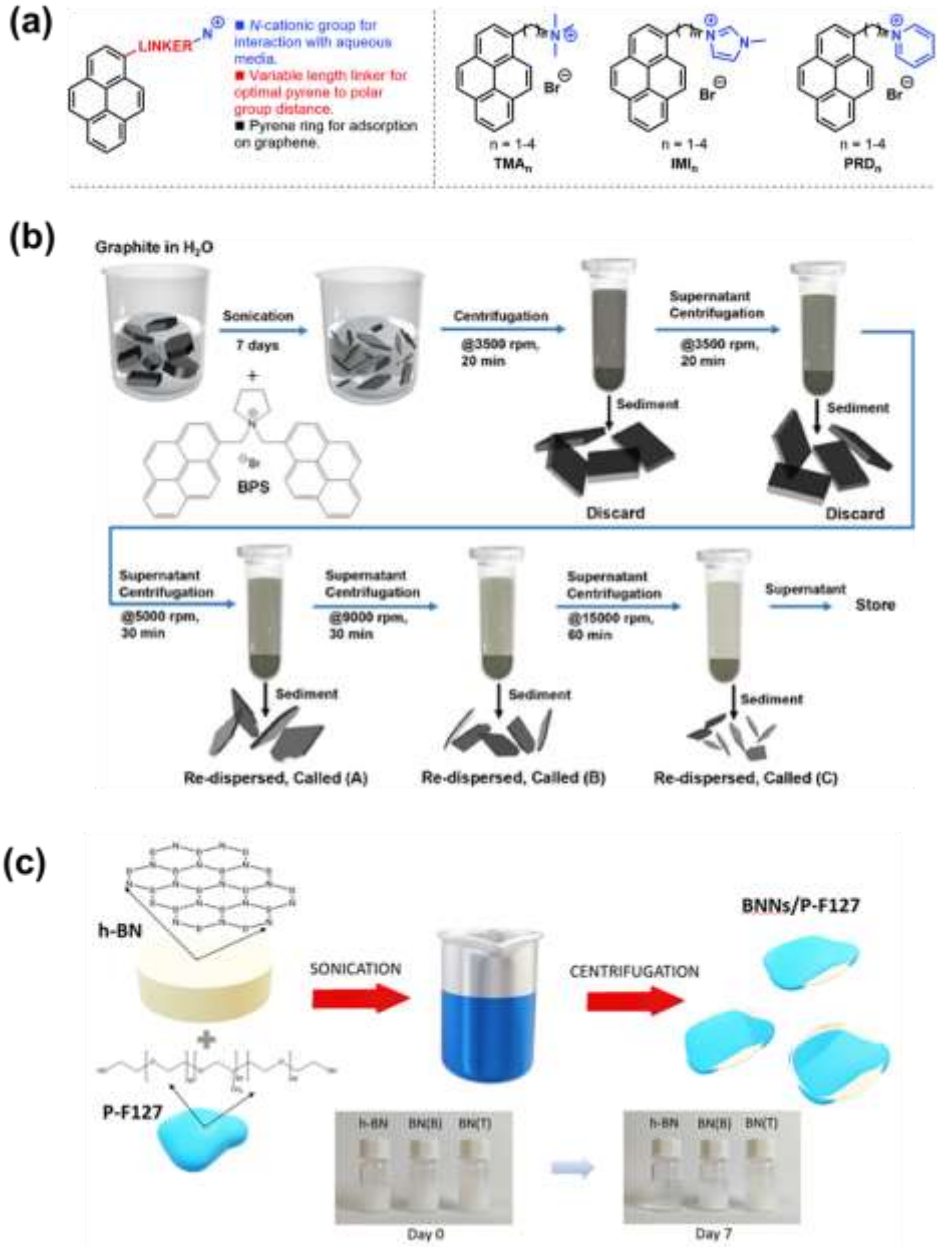

Figure 4. Chemical structures and processes of small aromatic molecules and surfactants for exfoliation of graphene and hBN. (a) Design of a series of cationic amphiphilic pyrene derivatives for the exfoliation of graphene. Reproduced with permission.[71] Copyright 2020, Royal Society of Chemistry. (b) Process of exfoliation of graphene with BPS and preparation of graphene in water with different size distributions by liquid cascade centrifugation. Reproduced with permission.[72] Copyright 2022, American Chemical Society. (c) Exfoliation of hBN in aqueous phase in the presence of Pluronic F127. Photos of the exfoliated hBN suspensions after 7 days. Reproduced with permission.[76] Copyright 2022, MDPI (2022).

4. Bioactive molecules

Many different bioactive molecules, including proteins, nucleotides, DNA, peptides, biomacromolecules, bile salts and other small molecules, have been explored to exfoliate 2DMs. Bioactive molecules possess many advantages compared to synthetic molecules, such as environmental friendliness, good biocompatibility and biodegradability.[85,86] In consequence, the obtained layered materials display a high biocompatibility, can find applications in biomedicine and are environmentally friendly.

4.1. Peptides and Proteins

Peptides have a high affinity for graphene. They can specifically recognize and bind to the basal plane or the edges of graphene via π–π stacking or electrostatic interactions.[87,88] Single-layer graphene can be prepared by exfoliation with amphiphilic peptides.[89,90] For instance, histidine-rich peptides with stearic acid and arginine amino acids at the terminal parts were used to exfoliate graphene, obtaining nanosheets with a lateral size of 150 nm.[91] No cytotoxic effects were observed on hamster ovary cancer CHO-K1 cells. The hydrophobic anticancer drug ellipticine was adsorbed on the peptide-exfoliated graphene. The uptake efficiency of the peptide-graphene-ellipticine complex in the CHO-K1 cells was ~30% higher than peptide-ellipticine.

Proteins are highly abundant in living organisms, from bacteria and plants to animals and humans. Bovine serum albumin (BSA) is one of the most abundant natural proteins with vital physiological functions. Structurally, it consists of 583 amino acid residues with 17 disulfide bridges and one free SH group.[92,93] The protein has been employed as an exfoliating reagent, as it contains hydrophilic and hydrophobic parts. For example, BSA has been used to exfoliate bulk MoS_2 by sonication.[85] Single-layer MoS_2 was obtained at a concentration less than 2 mg/mL. Density functional theory simulation suggested that the benzene rings and disulfides

in BSA were strongly bound on the layered MoS_2 due to a high binding affinity, while the polar groups were exposed to water, leading to an effective exfoliation. The single-layer MoS_2-BSA showed a higher cell viability on fibroblasts compared with PAA- and PVP-stabilized MoS_2 as well as bulk MoS_2. BSA-exfoliated MoS_2 has also been explored to load the chemotherapeutic drug resveratrol for cancer therapy (**Figure 5a**).[94] The BSA-MoS_2 nanosheets were stable in aqueous solution over one month, possessed a good biocompatibility and a high cellular uptake capacity. The heat generated by PTT triggered the release of resveratrol from the MoS_2 surface, thus promoting a therapeutic effect in tumor-bearing mice via NIR-induced hyperthermia and drug release. Graphite can also be exfoliated by ball milling using BSA as an intercalating agent.[95] The BSA-coated graphene showed a negligible cytotoxicity on astrocytes at a low concentration, but induced cell death at a higher concentration. The cytotoxicity mainly derived from residual endotoxins in BSA, as endotoxins can trigger inflammatory responses and further lead to a deleterious impact on cells. Therefore, endotoxin-free BSA was used to exfoliate graphene.[24] The endotoxin-free BSA-exfoliated graphene was less inflammatory than vaccine adjuvant alum after intraperitoneal injection. The endotoxin-free BSA-exfoliated graphene was engulfed by phagocytic cells and then accumulated in the lymphoid tissue. Serum is a complex mixture of proteins, peptides, amino acids and many other small molecules. In bovine serum, the amount of total proteins is 67.54 g/L, including 31.86 g/L of BSA and 35.68 g/L of globulin.[96] Interestingly, graphene has been successfully prepared using animal serum in a kitchen blender, where the protein content played an important role in the exfoliation process.[97] Six different animal sera (e.g., bovine, chicken, horse, human, porcine and rabbit) were used as exfoliating agents to produce few-layer graphene composed of three to four layers. The graphene dispersions were not toxic for H1299 human lung carcinoma cells and HEK-293T cells. It is worth noting that the few-layer graphene showed a size-dependent cytotoxicity, the smallest sample (< 200 nm) being more toxic than the larger sheets (500 nm). Besides, no acute toxic effects were induced on the *C. elegans* nematode worm model, which is an established model for developmental biology.

Silk fibroin, a protein produced by *Bombyx mori* silkworms, was also used to exfoliate 2DMs. The advantages of silk fibroin are its low price and large industrial production as well as good biocompatibility and degradability.[98] Silk nanofibers were used to exfoliate graphene at a high concentration (8 mg/mL) and with a large yield (30%).[99,100] The silk nanofiber-exfoliated graphene showed a negligible cytotoxicity after cultured with bone marrow-derived stem cells (BMSCs). The cell viability was 80% at the concentration of 60 μg/mL, which was much higher than graphene oxide. Silk fibroin, a protein found in the silk fibers, was also applied as an

exfoliating agent to separate TMD sheets. It was modified with carboxyl groups to avoid the inherent self-aggregation of silk fibroin during the exfoliation of $MoSe_2$ (**Figure 5b**).[101] The final concentration reached 1.98 mg/mL with a yield of 28.7%. The exfoliated $MoSe_2$ showed a peroxidase-like activity transforming H_2O_2 into hydroxyl radicals. Both Gram-negative *E. coli* and Gram-positive *B. subtilis* were destroyed by a film of the exfoliated $MoSe_2$. *In vivo* the exfoliated $MoSe_2$ effectively promoted wound healing in the presence of a low dose of H_2O_2.

In addition, lysozyme has been reported to efficiently exfoliate and disperse graphene in water.[102] Lysozyme is an antibacterial protein consisting of 129 residues rich in lysine and arginine. Due to the electrostatic interactions, the positively charged lysozyme can attach on the surface of graphene. The cytotoxicity of the lysozyme-graphene was evaluated on NIH-3T3 fibroblasts as well as three cancer cell lines (HCT-116, HeLa and SCC-7). The results showed that the lysozyme-graphene was more toxic to cancer cells than to fibroblasts, providing opportunities for cancer therapy. In alternative to lysozyme, calf histone, ovalbumin and bovine hemoglobin were selected for exfoliation. Ovalbumin-exfoliated graphene was less toxic compared to the calf histone and lysozyme-exfoliated graphene. The varying toxicities can be attributed to the distinct isoelectric points of the different proteins, causing positively charged graphene to exhibit a greater tendency for internalization compared to negatively charged graphene. In another study, a lysozyme derivative bearing aminopropyl moieties bound to the eight cysteine residues was designed and employed to produce MoS_2 nanosheets with a good stability in PBS and fetal bovine serum.[103] The cell viability was not affected up to 48 h and no changes in cell morphology was found. Besides, lysozyme is an antibacterial agent against both Gram-positive and Gram-negative bacteria. In a recent study, lysozyme-MoS_2 was investigated as an antibacterial agent (**Figure 5c**).[12] Bulk MoS_2 was first ball-milled and treated with H_2SO_4, followed by sonication in water in the presence of lysozyme. The cytotoxicity evaluation was first carried out on HUVEC cells showing a viability of more than 92 % at the highest concentration (100 μg/mL). The lysozyme-exfoliated MoS_2 possessed a high bactericidal efficacy against ampicillin-resistant *E. coli* and *B. subtilis*, likely due to the contribution of the high peroxidase-like catalytic activity and the antibacterial lysozyme as well as the mechanical action of the sharp edges of the MoS_2 sheets.

Apart from BSA, lysozyme and proteins from serum, other proteins extracted from natural products have also been investigated for LPE of 2DMs. For example, wool keratin, extracted from wool fibers, was used to exfoliate MoS_2 in aqueous solutions with a thickness of 3~4 nm.[104] The high content of cysteine (7–20 wt%) in wool keratin can bind to the edge defects, i.e. sulfur vacancies of MoS_2. Mouse osteoblast cells were seeded on exfoliated MoS_2, and the

increase of cell proliferation supported a good biocompatibility. In the same study, the exfoliation using wool keratin was extended to other 2DMs, such as WS_2, WSe_2 and $MoSe_2$. Besides, casein, a zwitterionic protein abundantly found in milk, was proved to exfoliate graphene in aqueous phase in the presence of ammonia.[105] The hydrophobic part of casein can tightly adsorb on the graphene layers, resulting in a high yield of exfoliation (21.4%). The casein-exfoliated graphene showed a low cytotoxicity on MLg cells. Since casein is often used as an emulsifier in various cosmetic preparations, casein-exfoliated graphene could be suitable in food and cosmetic fields.

Gelatin, a mixture of proteins and peptides extracted from animal skin and bone, has been widely investigated for biomedical applications and also used for the exfoliation of graphene.[106,107] Gelatin can interact with graphite via π–π stacking, resulting in a low surface tension that facilitates the exfoliation. Low defect graphene was obtained at a high concentration in water (4.37 mg/mL). The gelatin-exfoliated graphene showed a good cytocompatibility on HeLa cells even at a high concentration of 1 mg/mL and an excellent hemocompatibility on human red blood cells, with only ~2% hemolysis measured at a very high concentration of 10 mg/mL.

Overall, the exfoliation with proteins is an innovative approach that can provide few-layer 2DMs with high quality. The excellent biocompatibility of proteins can effectively reduce the potential toxicity of 2DMs. However, it is necessary to study in detail the interactions between proteins and 2DMs to better control the exfoliation process.

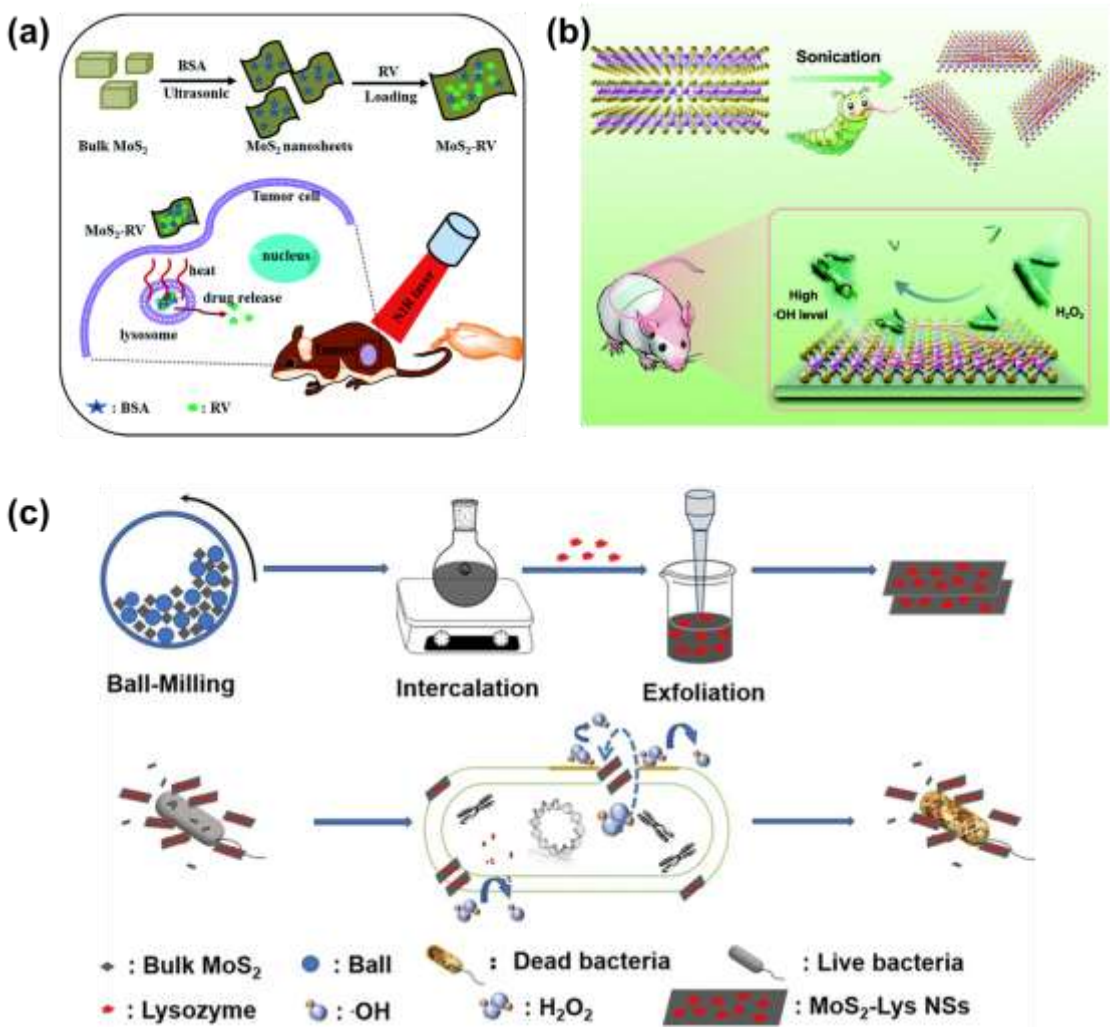

Figure 5. Protein-assisted exfoliation of TMDs for anticancer therapy, wound healing and antibacterial applications. (a) Exfoliation of MoS_2 by BSA and adsorption of resveratrol for NIR-controlled drug release and PTT. Reproduced with permission.[94] Copyright 2016, Royal Society of Chemistry. (b) Exfoliation of $MoSe_2$ in the presence of silk fibroin. The resulting nanosheets exhibited a peroxidase-like activity and were explored for wound healing *in vivo*. Reproduced with permission.[101] Copyright 2017, Royal Society of Chemistry. (c) Preparation routes of lysozyme-stabilized MoS_2, which was used to kill bacteria thanks to the peroxidase-like catalytic properties and antibacterial performance of lysozyme. Reproduced with permission.[12] Copyright 2020, Wiley-VCH.

4.2. Nucleotides

Nucleotides are small molecular intracellular compounds made up of three components: a nitrogen heterocyclic base (pyrimidine or purine), a pentose (deoxyribose or ribose) and one phosphate or polyphosphate group.[108] Flavin mononucleotide (FMN) is a derivative of riboflavin (vitamin B_2) that has been used as a dispersing agent. The isoalloxazine moiety

showed strong adsorption, while the negatively charged phosphate group in the structure provided an additional electrostatic interaction, leading to the successful exfoliation of graphene reaching a very high concentration of 50 mg/mL (**Figure 6a**).[109] The impact of the FMN-exfoliated graphene on the inflammatory and metabolic responses of macrophages was investigated.[110] The results showed that the uptake of the FMN-graphene in macrophages was dependent on the lateral size, with the smaller graphene nanosheets exhibiting a greater cellular internalization. Furthermore, a high production of nitric oxide and macrophage metabolites, such as succinate, itaconate, phosphocholine and phosphocreatine, was observed for both small and large graphene, indicating that the FMN-graphene induced macrophage pro-inflammatory responses. In another study, the cytotoxicity of the FMN-exfoliated graphene was studied on osteosarcoma and healthy cells.[111] The viability of Saos-2 tumor osteoblasts and MC3T3-E1 undifferentiated preosteoblasts was 80% and 40%, respectively, after incubation with the FMN-graphene at a concentration of 50 μg/mL, showing a notable impact on the preosteoblasts. The main causes of cytotoxicity were due to the oxidative stress through ROS production leading to apoptosis. In another study, the toxicology of few-layer graphene obtained by exfoliation using riboflavin-5′ -phosphate sodium salt (Rib) was assessed using two cell culture models and a healthy murine model.[112] After 24 h incubation with Rib-exfoliated graphene (G-Rib) at a high concentration of 300 μg/mL, no sign of toxicity was observed on HeLa cells and RAW 264.7 macrophages. After intravenous injection of G-Rib in Balb/c mice, G-Rib was found to accumulate in the liver and spleen, while some sheets were eliminated from the body by urinary excretion through the kidney. No obvious pathological changes were detected in the main organs, such as liver, kidneys, lung and spleen, up to 30 days. Moreover, G-Rib showed a low hematotoxicity and no inflammation. These studies demonstrate the high biocompatibility of riboflavin-exfoliated graphene, giving a great promise as a potential candidate for biomedical application.

Other nucleotides have also been proved efficient dispersants for the exfoliation of TMDs in water due to the specific nucleotide-flake interactions based on Lewis acid–base interactions.[113, 114] Deoxyadenosine monophosphate (AMP), deoxyguanosine monophosphate (GMP), deoxythymidine monophosphate (TMP) and deoxycytidine monophosphate (CMP), are four nucleotides of DNA and have been used for the exfoliation of MoS_2. No toxicity of the MoS_2 exfoliated by the different nucleotides towards MC3T3-E1 preosteoclasts and human Saos-2 osteoblasts was observed.[115] Moreover, the high activity of the alkaline phosphatase indicated that the dispersed MoS_2 showed a negligible effect at the early stage of the preosteoclast differentiation. However, the weak absorption between DNA nucleotides and the surface of

2DM generally leads to a low exfoliation efficiency. To address this issue, the combination of a nucleotide with its complementary nucleobase has been demonstrated as a more efficient strategy to exfoliate graphene thanks to the supramolecular interactions between the nucleobases.[114] During the exfoliation, the nucleotides and nucleobases adsorb on the surface via π–π interactions and bound to each other through hydrogen bonds to form supramolecular entities. The cytotoxicity of graphene exfoliated by AMP-thymine was investigated on L-929 cells. Although the proliferation of the cells on the AMP-thymine graphene films was slow in the first 2 days, a steady increase of the proliferation up to 75% was observed after 7 days, revealing a good biocompatibility.

DNA-exfoliated TMDs have been explored for antibacterial and antitumor effects. Single-stranded DNA (ssDNA) was used to exfoliate WX_2 (X = S, Se).[116] The hydrogen bridges between the primary amines in adenine, guanine and cytosine or oxygen atoms of the ssDNA and the surface or defective edges of WX_2 led to high exfoliation yields. Compared to WS_2-ssDNA and GO, WSe_2-ssDNA showed a higher antibacterial capacity against *E. coli* with 82.3% loss of cell viability, likely due to the induction of a ROS-independent oxidative stress. Besides, DNA-exfoliated $NbSe_2$ prepared by cryo-pretreatment by immersion in liquid nitrogen for 1 h was explored for anti-inflammatory and antitumor treatment (**Figure 6b**).[117] The capability of the DNA-exfoliated $NbSe_2$ for the elimination of reactive oxygen and nitrogen species (RNOS) was studied by computational simulations, revealing that the $NbSe_2$ nanosheets could scavenge RNOS via a hydrogen atom transfer and a redox reaction. The exfoliated $NbSe_2$ downregulated inflammatory cytokines, like TNF-α and IL-6, *in vitro* and *in vivo*, further protecting the normal cells against oxidative damage. With the precise guidance of PAI, a U87 tumor was ablated by PTT in mice, while no inflammation triggered by the photothermal treatment was observed.

In general, the use of nucleotides as exfoliation agents has not been extensively studied. Nucleotides, represented by FMN, offer the possibility to produce a large scale of 2DMs. Additionally, owing to the biological relevance of nucleotides, 2DMs exfoliated by nucleotides may have potential applications as biofunctionalized materials.

4.3. Small bioactive molecules

Bile acids are steroids existing in many vertebrates, where they are synthesized in the liver. They are obtained by conjugation of bile acids with taurine or glycine and possess a hydrophilic part due to the hydroxyl and carboxylate groups, as well as a hydrophobic part contributed by the tetracyclic carbon backbone (**Figure 6c**). Because of their amphiphilicity, bile salts have

been extensively utilized to exfoliate and stabilize 2DMs.[118] Graphene dispersions can be stabilized in water by sodium cholate, a type of bile salts, at a concentration of 0.3 mg/mL.[119] Using a low power and long sonication time, stable dispersions containing ~10% of monolayer sheets can be obtained. Few-layer graphene obtained by exfoliation of graphite using sodium cholate, showed a slight toxicity on RAW 264.7 macrophages at the highest dose of 120 μg/mL.[120] The exfoliated graphene induced the secretion of cytokines (TNF-α and IL-6) and produced NO and ROS. Interestingly, no secretion of other cytokines (IL-1β and IL-18) was found, indicating that the inflammasome, the innate immune system receptors and sensors responsible of inflammatory responses, was not activated. The few-layer graphene was internalized by macrophages inducing inflammation via oxidative stress, followed by activation of autophagy. This pathway can protect the cells from excess inflammation. In another study, the cytotoxicity, cellular uptake and catabolic pathways of bile salt-exfoliated graphene were investigated.[121] No cytotoxicity on primary macrophages was found and the exfoliated graphene was catabolized by the lysosomal pathway.

LPE using sodium cholate was applied to other 2DMs, such as MoS_2, WS_2, $MoTe_2$, $MoSe_2$, $NbSe_2$, $TaSe_2$ and hBN, to produce defect-free sheets with a lateral size of hundreds of nanometers.[122] Monolayer WS_2 showed antibacterial properties; indeed, the viability of *E. coli* and *S. aureus* decreased below 5% at a concentration of 100 μg/mL.[123] Besides, WS_2 sheets were found to be non-cytotoxic on A549 and HepG2 cells at a low concentration (25 μg/mL). As the concentration increased, the cell viability of A549 and HepG2 decreased gradually, and WS_2 sheets showed higher toxicity in A549 cells than in HepG2 cells. In another study, sodium cholate-exfoliated MoS_2 sheets with different lateral size distributions (50, 117 and 177 nm) were prepared by LPE and liquid cascade centrifugation.[124] Their cellular uptake, cytotoxicity as well as inflammatory response were investigated on three cell lines (THP-1 leukemia monocytic cells, A549 and AGS gastric cancer cells). Independently of their size the MoS_2 sheets were internalized by cells into vesicles, and were not toxic at the concentration of 1 μg/mL. At higher concentration (10 μg/mL), MoS_2 elicited higher cytotoxicity on THP-1 cells and lower cytotoxicity on A549 and AGS cells. Interestingly, the cytokine response in THP-1 macrophages showed a size-dependent effect, the smaller MoS_2 sheets inducing a higher production of cytokines. This effect is likely due to the decrease of the sheet size. Indeed, since the endotoxin is bound to the edges, smaller sheets offer a greater number of accessible surface edges for endotoxin attachment, which can cause an inflammatory response. Besides, our group evaluated the inflammatory status of the lungs in healthy mice after inhalation of sodium cholate-exfoliated MoS_2 nanosheets.[125] The material induced acute lung inflammation, which

was subsequently resolved within a few days and led to the sustained resolution of inflammation. With the help of liquid phase transmission electron microscopy, it was suggested that MoS_2 underwent three distinct transformations by intracellular ROS, corresponding to the formation of MoS_2 nanoscrolls, etching with release of degradation products and generation of oxidized fragments. In another work from our group, the interactions between sodium cholate-exfoliated hBN and cell membrane was studied by molecular dynamics simulations and *in vitro* studies.[126] Two sources of hBN were used: round hBN (r-hBN) and cornered hBN (c-hBN). *In vitro* experiments demonstrated that c-hBN was toxic on lung epithelial H460 lung epithelial cells at the highest concentration (80 μg/mL), whereas r-hBN showed negligible cytotoxicity. c-hBN induced a lysosomal membrane permeabilization leading to cell death. Molecular dynamics simulations suggested that c-hBN could cross the cell membrane forming hydrophilic water channels, which are responsible of lysosomal membrane permeabilization and cell death. Renewable and nontoxic small molecules, such as carbohydrates, have been also investigated as exfoliating agents of 2DMs for potential biomedical applications.[127] Glucose, fructose and saccharose were used to exfoliate graphene through ball milling, followed by centrifugation and dialysis to purify the obtained sheets. Glucose-stabilized graphene resulted made of 2~3 layers with an average size of 120 nm. The glucose-graphene showed a lower toxicity on HaCaT cells. In another study, sodium phytate, a sodium salt form phytic acid extracted from rice bran, has been explored for the exfoliation of MoS_2 (**Figure 6d**).[128] The layered MoS_2 was obtained at a concentration of 1 mg/mL and 18.1% yield (8 times higher than the exfoliation in pure water). The high exfoliation efficiency of sodium phytate was attributed to the six phosphate groups in the molecule, able to insert between the layers of MoS_2 to facilitate the exfoliation process. The MoS_2 nanosheets showed a negligible cytotoxicity on HepG2 liver cancer cells at concentrations up to 250 μg/mL. The sulfur atoms showed a strong and specific interaction with Hg^{2+}, while the phytate on the surface also contributed to chelate this heavy metal. *In vitro* studies confirmed the elimination of Hg^{2+} from poisoned HepG2 cells, indicating the potential use of sodium phytate-exfoliated MoS_2 as detoxificant.

Among all the small molecules discussed above, sodium cholate showed good efficacy for the exfoliation of 2DMs. However, the potential toxicity of the exfoliated materials and how they might induce toxic effects, as well as their bioapplications still need further investigation.

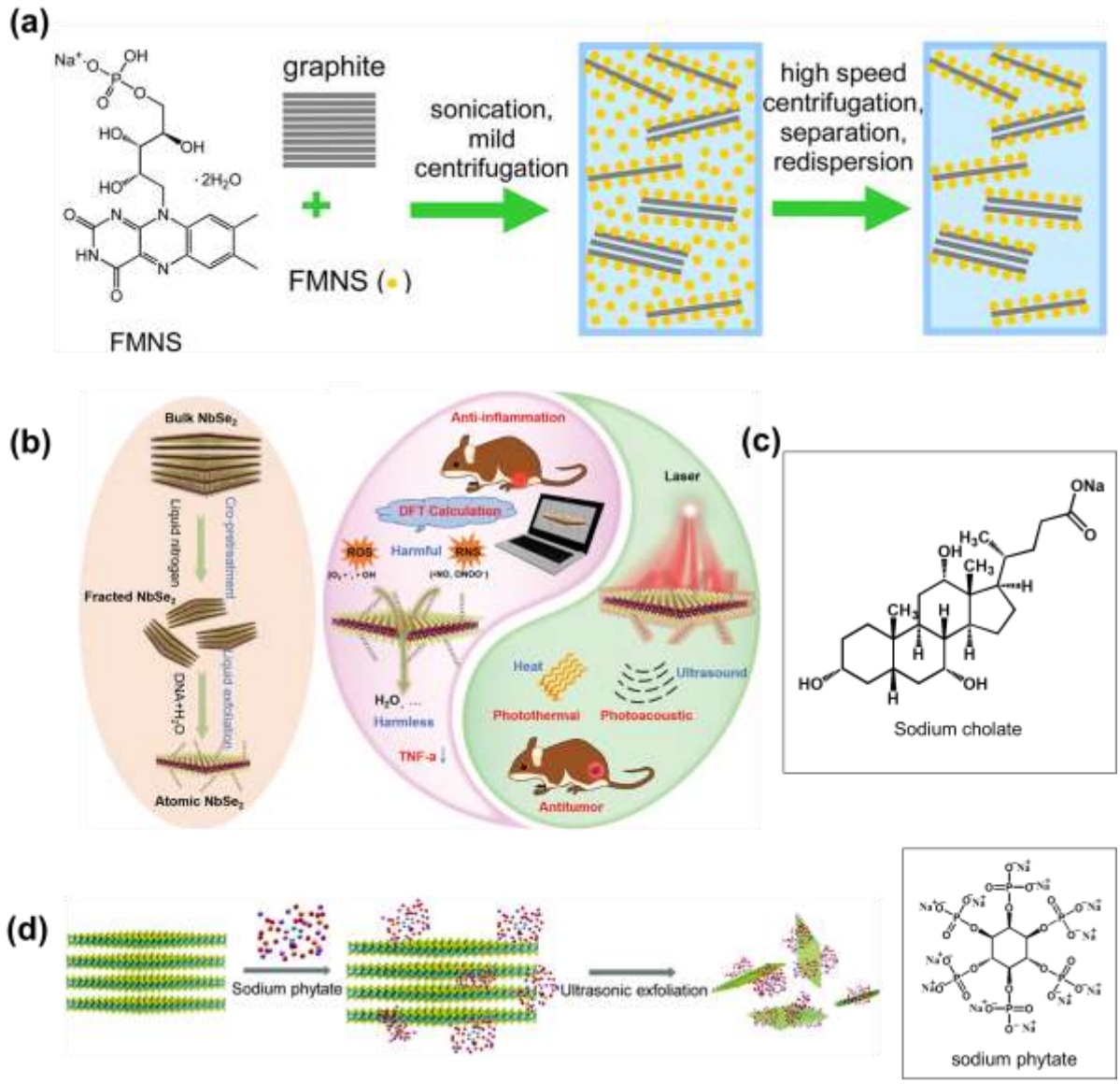

Figure 6. Graphene and TMDs exfoliated with nucleotides and small bioactive molecules for bioapplications. (a) Schematic illustration of LPE using graphite and FMN sodium salt (FMNS). Reproduced with permission.[109] Copyright 2015, American Chemical Society. (b) Exfoliation and functionalization of $NbSe_2$ using DNA for anti-inflammation and antitumor therapy *in vivo*. Reproduced with permission.[117] Copyright 2020, Wiley-VCH. (c) Chemical structure of sodium cholate. (d) Ultrasonic exfoliation of MoS_2 using sodium phytate. Reproduced with permission.[128] Copyright 2022, Royal Society of Chemistry.

4.4. Biomacromolecules

Natural biomacromolecules, such as chitosan, lignin, cellulose, sodium alginate and hyaluronic acid, have attracted a high attention in biomedicine due to their biosafety, biocompatibility and long blood circulation.[129] Several studies have focused on the exfoliation directly using these natural biomacromolecules.[130,131] Positively charged chitosan-exfoliated MoS_2 with an

average size of 126 nm was obtained by ultrasonication in aqueous solution.[132] Through the membrane disruption mediated inactivation and oxidative damage, chitosan-MoS_2 inhibited 96% and 98% of the growth of ampicillin resistant *E. coli* and *S. aureus* at the concentrations of 60 μg/mL and 120 μg/mL, respectively. The chitosan-MoS_2 also showed a low cytotoxicity on MCF-7 cancer cells and HEK-293A normal kidney cells up to 200 μg/mL. Another method based on oleum pretreatment was explored to improve the exfoliation efficiency of MoS_2.[25] The oleum was initially used to exfoliate MoS_2 at 90°C, followed by its removal through centrifugation and washing and subsequent exfoliation in aqueous phase using chitosan. The chitosan-exfoliated MoS_2 was investigated as a photothermal induced-drug delivery platform for cancer therapy. Chitosan-MoS_2 showed a higher cytocompatibility than MoS_2 obtained from oleum treatment on KB epidermoid carcinoma cells and PANC-1 human pancreatic cancer cells, as well as a good biocompatibility based on hemolytic experiments. Chitosan-MoS_2 inhibited the tumor growth *in vivo* through the combination of hyperthermia and chemotherapy, while it showed the potential to be used as a CT contrast agent for imaging *in vitro*. In another study, chitosan was employed to exfoliate graphene by ball-milling for intraocular electrode application to detect glucose.[133] Chitosan-graphene exhibited a good ocular biocompatibility with around 100% and 80% cell viability on circulating endothelial cells (CECs) and retinal pigment epithelium (RPE) cells, respectively, at a concentration of 100 μg/mL. The wearable contact electrodes were tested on rabbits to monitor the intraocular blood sugar in tears, and no obvious congestion and inflammation were observed, indicating a high biocompatibility and great potential for curing eye diseases.

Overall, these studies demonstrate that bioactive molecules are powerful tools serving as effective exfoliating agents to produce layered 2DMs with a good colloidal stability in aqueous media. Their high biocompatibility allows their direct use for cancer therapy and antibacterial applications.

5. Conclusions

2DMs can be easily exfoliated by LPE to layered sheets with a great potential for biomedical applications. Extensive studies have focused on the use of exfoliated 2DMs for drug delivery, antitumor therapy, as well as antimicrobials and biosensors. Therefore, the choice of the exfoliation method is crucial to meet the specific needs for a targeted application. Surfactant-free exfoliation provides a simple way to produce 2DMs in organic and/or aqueous phase. However, the surface residual organic solvents might induce a risk of toxicity. Although the exfoliation of BP can be easily achieved by LPE in pure water to minimize any potential impact

of the absorbed molecules on subsequent chemical modifications and avoid any risk of toxicity associated with the exfoliating agents, other 2DMs can hardly be exfoliated in pure water. Therefore, when it comes to graphene, TMDs and other 2DMs, the exfoliation in mixed aqueous and organic phases gives an alternative promising approach. Unnatural molecules, such as aromatic molecules and polymers, have been employed to improve the stability of the suspensions. Exfoliation with aromatic molecules can result in a high yield, but the biosafety of the exfoliated sheets needs to be verified. Biocompatible polymers could be another choice to achieve favorable biosafety. Bioactive molecules, such as peptides, DNA and proteins, can adsorb onto the surface of 2DMs through various interactions and prevent the material from re-aggregation. Considering the intrinsic low toxicity and abundant natural sources, the exfoliation of 2DMs with bioactive molecules leads to suspensions with an increased biocompatibility compared to materials exfoliated using non-natural synthetic molecules.

The evaluation of the biocompatibility of 2DMs obtained by LPE is essential for guiding their bioapplications. Many *in vitro* studies have provided valuable insights on cellular uptake, cytotoxicity, cellular response, and degradation, while *in vivo* studies can bring understanding on biosafety and potential toxicity, immune response, therapeutic efficacy and long-term effects on living organisms. Nevertheless, more investigations are needed to draw general conclusions about the biocompatibility of 2DMs, for instance the biodistribution, clearance, degradation and potential immune response should be investigated in animal models. Noteworthy, the size, thickness, shape and surface functional groups can influence the toxicity of 2DMs. Therefore, controlling these parameters during LPE can help modulating the biocompatibility of 2DMs, while further functionalization can minimize the potential toxicity and impart novel properties, for example for targeting specific cells, therapy and imaging.

In summary, LPE is a simple and powerful technique to produce layered materials. By carefully selecting the exfoliating agents, LPE can yield exfoliated 2DMs with a great potential for biomedical applications. Importantly, there is still room to explore other types of exfoliating agents and investigate the biocompatibility and biomedical applications of 2DMs.

Table 1. Reported 2DMs by LPE and their biocompatibility and bioapplications.

Exfoliating agent/solvent	2DMs	Average size & thickness	Concentration & yield	Biocompatibility	Bioapplications	Ref. (Year of Publication)

NMP	BP	100-400 nm; 5-8 nm	-	*In vitro* cytotoxicity of 4T1 and MCF-10A cells	*In vivo* fluorescence imaging; *in vivo* PTT and chemotherapy	**Erreur ! Signet non défini.** (2020)
NMP	BP	50-430 nm; 5.1-10.8 nm	-	Toxicity assay on B16, SMMC-7721, and J774A.1 cells	*In vitro* and *in vivo* PTT	31 (2018)
NMP	BP	several hundred nm; 3-5 nm	-	*In vitro* cytotoxicity on PC12 cells	*In vitro* Alzheimer's disease therapy	32 (2019)
NMP	BP	100 nm; 8-12 nm	-	*In vitro* cytotoxicity on L929, 4T1 and B16 cells	*In vitro and in vivo* photo-immunotherapy	33 (2020)
NMP	BP	330 nm; 2.1 nm	-	*In vitro* cytotoxicity on 4T1 cells	*In vitro and in vivo* PTT	34 (2019)
NMP	BP	220 nm; 1 nm	-	*In vitro* cytotoxicity on MCF-7 cells	*In vitro and in vivo* PTT and gene therapy	35 (2018)
NMP	MoS_2	101 nm; -	-	*In vitro* cytotoxicity on HepG2 cells	*In vitro and in vivo* CDT; *In vivo* PAI and MRI	36 (2021)
NMP	WS_2	150 nm; -	-	*In vitro* cytotoxicity on HepG2 cells and biocompatibility on zebrafish	*In vitro* PTT	37 (2021)
DMF	MoS_2	-; 2–3 layers	-	*In vitro* cytotoxicity and electrical impedance analysis on RAMEC cells and PC12 cells	-	38 (2015)
DMSO	BP	394 nm, 118 nm and 4.5 nm; 15–18 nm, 6–7 nm and 2–3 nm	-	*In vitro* cytotoxicity on LO2 cells	*In vitro* PTT on MCF-7 cells	39 (2017)
2-Butanone	MoS_2	246 nm (1000 rpm), 177 nm (2000 rpm), 141 nm (3000 rpm), 134 nm (4000 rpm)	1 mg/mL	*In vitro* cytotoxicity on mixed glial cells;	-	23 (2021)

		and 95 nm (5000 rpm); 10–14 layers (1000 and 3000 rpm), 6–7 layers (4000 and 5000 rpm)		Enzymatic degradability with human myeloperoxidase		
2-Butanone	hBN	532 nm (1000 rpm), 376 nm (2000 rpm), 240 nm (3000 rpm) and 141 nm (5000 rpm); 18 layers (1000 rpm), 3 layers (5000 rpm)	1 mg/mL	*In vitro* cytotoxicity on mixed glial cells; Enzymatic degradability with human myeloperoxidase	-	23 (2021)
IPA	BP	150 nm; 7.2 nm (10–12 layers)	-	*In vitro* cytotoxicity on Huh7 cells, HepG2 cells and HeLa cells; *In vivo* toxicity in mice; *In vitro and in vivo* PTT	-	43 (2020)
IPA	BP	100-200 nm; 4 nm	-	*In vitro* and *in vivo* capture of CTC and PTT	*In vitro* and *in vivo* PTT	44 (2020)
DMPU	BP	100 nm–4 μm; 2.0 to 15.4 nm	1.1 mg/mL; 16%	*In vitro* cytotoxicity on HeLa cells	*In vitro* PTT antibacterial activity on *E. coli* and *S. aureus*	45 (2018)
Cyclopentanone	MoS_2	200 nm; 8 layers	-	Internalization and location in U2OS cells and 1BR primary fibroblasts	-	48 (2021)
Water	BP	Several hundred nm; 2.0 nm (4 layers)	0.02 mg/mL	*In vitro* cytotoxicity on MDA-MB-231 cells	*In vitro* and *in vivo* PDT on MDA-MB-231 cells	53 (2015)
Water	BP	884.0 nm, 425.5 nm, and 208.5 nm; 91.9 nm, 27.0 nm, and 17.4 nm	-	*In vitro* toxicity on NIH 3T3, HCoEpiC, and 293T cells; Intracellular ROS generation on NIH 3T3 cells	-	54 (2017)

Water	BP	120 nm; 1-2 nm	200 μg/mL	*In vitro* cytotoxicity on HeLa cells	*In vitro* and *in vivo* PTT and chemotherapy on HeLa cells	55 (2017)
Water	BP	960 nm; 6.87 nm	-	*In vitro* cytotoxicity on L929 cells; hemolysis test	*In vitro* and *in vivo* PDT and PTT; *In vivo* T_2 MRI	56 (2017)
Water	MoS_2	76.7 nm; 5 layers	124 μg/mL	*In vitro* cytotoxicity and cellular uptake on JIMT-1 and MRC5	Confocal Raman imaging on JIMT-1 cells	59 (2020)
Water	MoS_2	0.88 μm; 3.1 nm	-	Toxicity on beneficial soil bacteria *B. cereus* and *P. aeruginosa*	-	60 (2021)
Water	MoS_2	76 nm; 2 layers	10 μg/mL	*In vitro* cytotoxicity on U937, MCF-7 and HaCaT	*In vitro* antibacterial activity on *Salmonella ATCC 14028* and wild-type *Salmonella*	61 (2018)
Water (oleum pretreatment)	MoS_2	80 nm; 4 nm	-	*In vitro* cytotoxicity on HUVEC cells and SMMC-7721 cells; *in vitro* endocytosis and exocytosis; *in vitro* biodegradability and *in vivo* biodistribution; hematological and histological analyses	-	62 (2019)
45% (v/v) ethanol/water	MoS_2	77 nm; 3.4 nm	0.1 mg/mL	*In vitro* cytotoxicity on SKM-1 cells	Targeting the SKM-1 cells for diagnosis of acute myeloid leukemia	65 (2021)
1-Pyrene-sulfonic acid in water	WS_2	50 nm; 7 nm (7 layers)	-	*In vitro* cytotoxicity, cellular uptake and endotoxin assessment on A549 and HaCaT cells;	Triggering trained immunity on human monocyte-derived macrophages	70 (2022)

Cationic pyrene derivatives/water	Graphene	200 nm; 2-10 nm	0.4 mg/mL	*In vitro* cellular uptake and cytotoxicity on BEAS-2B and HeLa cells	-	71 (2020)
Pyrene derivative/water	Graphene	GR0.3: 187.9 nm; 6.2 nm GR0.4: 200.1 nm; 6.9 nm GR0.6: 229.8 nm; 7.9 nm GR1.0: 195.5 nm; 7.5 nm	> 0.5 mg/mL	*In vitro* cytotoxicity on BEAS-2B cells	-	72 (2022)
CTAB/water	Graphene	1.5 μm and 500 nm; 4 layers	-	-	*In vitro* antibacterial activity on *S. aureus* and *P. aeruginosa*	73 (2015)
Pluronic L64 and F108/water	Graphene	344.3 nm; < 3 nm	-	*In vitro* cytotoxicity on NG108-15 cells	*In vitro* PTT on NG108-15 cells	75 (2018)
Pluronic F127/water	BN	116.0 nm (bath sonication); 77.5 nm (tip sonication); 6-8 nm	1.5 mg/mL; 28.0% (tip sonication); 27.2% (bath sonication)	*In vitro* cytotoxicity and cellular uptake on HeLa cells	-	76 (2022)
PVP/water	Graphene	70 nm; 2 nm	22 μg/mL; -	*In vitro* cytotoxicity on U251cells	*In vitro* PTT on U251 cells	80 (2011)
PVP/water/ethanol	MoS_2	30-120 nm; 2 nm (3-4 layers)	-	*In vitro* cytotoxicity on U251 cells	*In vitro* PTT on human U251 cells; cell-targeted imaging	81 (2014)
Vinylimidazole-based polymers in water	Graphene	500 nm to 5 μm; 1.1-2.9 nm	1.12 mg/mL; 3%	*In vitro* cytotoxicity on L-929 cells	-	82 (2016)
Polyglycerol/water	Graphene	123 nm; -	3.2 mg/mL	*In vitro* cytotoxicity and cellular uptake on MCF-7 cells	*In vitro* PTT on MCF-7 cells	83 (2018)
Poly(acrylic acid)/water	Graphene	-; 2–6 layers	-	*In vitro* cytotoxicity on MG-63 cells	-	84 (2018)

Peptide/water	Graphene	100–500 nm; <5 nm	50 μg/mL; 82%	*In vitro* cytotoxicity and cellular uptake and cytotoxicity on CHO-K1 cells	*In vitro* cancer drug ellipticine uptake on CHO-K1 cells	91 (2019)
BSA/water	MoS_2	100 × 120 nm; 0.65 nm	1.36 mg/mL; 27.2%	*In vitro* cytotoxicity on fibroblast cells	-	85 (2015)
BSA/water	MoS_2	40–150 nm; 5–15 nm	-	*In vitro* cytotoxicity on Raji cells	*In vitro* and *in vivo* PTT and chemotherapy	94 (2016)
BSA/water	Graphene	19.89 nm ~ 14.56 nm	-	*In vitro* cytotoxicity on astrocyte cells	-	95 (2021)
BSA/water	Graphene	417 nm	-	*In vitro* cytotoxicity and cytokine secretion on bone marrow derived dendritic cells (BMDCs) and bone marrow-derived macrophages; *in vivo* cytokine secretion and inflammatory responses	-	24 (2018)
Serum/water	Graphene	Ultrasonication: ~ 0.5 μm length ~ 5 layers Kitchen blender: 0.5–1 μm; 3.5–4.4 layers Shear reactor: 1.1–1.6 μm; 5.8–6.9 layers	-	*In vitro* cytotoxicity on H1299 and HEK-293T cells; *In vivo* toxicity on *C. elegans*		97 (2017)
Silk nanofiber in water	Graphene	100–800 nm; 1–4 nm	8 mg/mL; 30%	*In vitro* cytotoxicity on BMSCs	-	99 (2018)
Silk nanofiber in water	Graphene	200–500 nm; 2 nm	1.92 mg/ mL; 20%	*In vitro* cytotoxicity on BMSCs	-	100 (2018)
Silk nanofiber/water	$MoSe_2$	100 nm; 1.0 nm	1.98 mg/mL; 28.7 %	*In vitro* cytotoxicity on L02 cells	*In vitro* and *in vivo* toxicity on *E. coli* and *B. subtilis*	101 (2017)
Lysozyme/water	Graphene	200 nm; 1.2 nm	2.09 mg/mL; -	*In vitro* cytotoxicity on NIH-3T3, HCT-	-	102 (2014)

				116, SCC-7 and HeLa cells		
Lysozyme/sodium acetate aqueous solution	MoS_2	250–550 nm; 5 nm	0.43 mg/mL; -	*In vitro* cytotoxicity on HeLa and HaCaT cells	-	103 (2017)
Lysozyme/H_2SO_4/ water	MoS_2	80–110 nm; -	1.0 mg/mL; 60%	*In vitro* cytotoxicity on HUVEC cells;	*In vitro* antibacterial activity on ampicillin-resistant *E. coli* and *B. subtilis*	12 (2020)
Wool keratin/water	MoS_2	100 nm; 3–4 nm	-	*In vitro* cytotoxicity on osteoblast cells	-	104 (2018)
Casein/water/ ammonia	Graphene	400 nm; < 8 nm	2.14 mg/mL; 21.4%	*In vitro* cytotoxicity on MLg cells	-	105 (2020)
Gelatin/water	Graphene	354 nm; 5 layers	4.37 mg/mL; 43.7 %	*In vitro* cytotoxicity on HeLa cells and hemocompatibility study	-	107 (2018)
Riboflavin/water	Graphene	Large: 200–400 nm; Small:100–200 nm	-	*In vitro* cell uptake, nitric oxide production and macrophage metabolome on RAW 264.7 macrophages	-	110 (2020)
Riboflavin/water	Graphene	840 nm; 5 layers	2 mg/mL; 2.5 wt%	*In vitro* cytotoxicity on RAW 264.7 and HeLa cells; *in vivo* toxicity and biodistribution	-	112 (2020)
DNA nucleotides (AMP, GMP, TMP and CMP)/water	MoS_2	200–400 nm; 5–9 nm 100–200 nm; 2–4 nm	5–10 mg/mL; -	*In vitro* cytotoxicity and proliferation on MC3T3-E1 and Saos-2 cells	-	113 (2017)
Nucleotide + nucleobases/water	Graphene	100–500 nm; 9–10 layers	1–2 mg mL; -	*In vitro* cytotoxicity on L-929 cells	Hydrogels for uptake and release of drugs and dyes	114 (2018)

Nucleotides (AMP, GMP and FMN)/water	MoS_2	250–300 nm; 9–10 layers	-	*In vitro* cytotoxicity, incorporation and differentiation on MC3T3-E1 and Saos-2 cells	-	115 (2019)
ssDNA/water	WS_2	65–650 nm; 1.4–2.6 nm	0.87 mg/mL; 80%–90%	-	*In vitro* antibacterial activity on *E. coli*	116 (2016)
ssDNA/water	WSe_2	64–550 nm; <10 nm	0.81 mg/mL; 80%–90%	-	*In vitro* antibacterial activity on *E. coli*	116 (2016)
Salmon sperm DNA/water	$NbSe_2$	50–150 nm; 1.36–2.14 nm	0.32 mg/mL; -	*In vitro* cytotoxicity on HUVEC; hemolysis test;	*In vitro* anti-inflammation on RAW-264.7 macrophages; *in vivo* anti-inflammation on lipopolysaccharide-induced rear thigh inflammation mouse models; *in vivo* PAI and antitumor therapy on U87 tumor-bearing mice	117 (2020)
Sodium cholate/water	Graphene	265 nm; 27 nm (~8 layers)	2.5 mg/mL; -	*In vitro* cytotoxicity, cytokine secretion, NO and ROS production on RAW-264.7 macrophages	-	120 (2018)
Sodium cholate/water	Graphene	500 nm; -	-	*In vitro* cytotoxicity, cellular uptake and catabolic pathways on primary macrophages	-	121 (2016)
Sodium cholate/water	WS_2	-; ~1 nm (2–3 layers)	-	*In vitro* cytotoxicity on A549 and HepG2 cells	*In vitro* antibacterial activity on *E. coli* and *S. aureus*	123 (2017)

Sodium cholate/water	MoS_2	50 nm, 117 nm and 177 nm -	-	*In vitro* cytotoxicity and cytokine secretion on THP-1, A549, AGS and BMDCs	-	124 (2017)
Sodium cholate/water	MoS_2	50-150 nm	-	Assessment of oxidative stress and inflammation *in vitro* on THP-1 monocytes; *in vivo* inflammatory status of the lung in healthy mice	-	125 (2023)
Sodium cholate/water	BN	c-hBN: 342 nm; 4.69 nm; r-hBN: 156 nm; 6-35 nm	1 mg/mL; -	*In vitro* cytotoxicity on H460 cells; *in vitro* superoxide anion quantification on H460 cells	-	126 (2021)
Carbohydrates/water	Graphene	120 nm; 2–3 layers	0.2 mg/mL; 47%	*In vitro* cytotoxicity on HaCaT cells	-	127 (2018)
Sodium phytate/water	MoS_2	90 nm; < 2 nm (2-3 layers)	1 mg/mL; 18.1%	*In vitro* cytotoxicity on HepG2 cells	*In vitro* and detoxification experiments on HepG2 cells	128 (2022)
Chitosan/water	MoS_2	126 nm; -	-	*In vitro* cytotoxicity on MCF-7 and HEK-293A cells	*In vitro* antibacterial activity and antibiofilm activity on *E. coli* and *S. aureus*	132 (2019)
Chitosan/water (oleum treatment)	MoS_2	80 nm; 4-6 nm	1 mg/mL; 79 %	*In vitro* cytotoxicity on KB and PANC-1 cells; hemolytic analysis; *in vivo* biocompatibility	*In vitro* and *in vivo* PTT on PANC-1 cells; *in vitro* PTT and chemotherapy on PANC-1 bearing mice	25 (2014)
Chitosan/water	Graphene	-; 0.75 nm	-	*In vitro* ocular biocompatibility on CECs and RPE cells	*In vivo* detection of glucose using intraocular biosensors	133 (2020)

Acknowledgements

This work was supported by the European Commission through the Graphene Flagship project (grant agreement no. 881603), by the Centre National de la Recherche Scientifique (CNRS), by the Interdisciplinary Thematic Institute SysChem, via the IdEx Unistra (ANR-10-IDEX-0002) and by the CSC Graduate School (CSC-IGS ANR-17-EURE-0016) within the French Investments for the Future Program. Y. He is indebted to the Chinese Scholarship Council for supporting her PhD internship.

Received: ((will be filled in by the editorial staff))

Revised: ((will be filled in by the editorial staff))

Published online: ((will be filled in by the editorial staff))

References

[1] K. S. Novoselov, A. K. Geim, S. V. Morozov, D. Jiang, Y. Zhang, S. V. Dubonos, I. V. Grigorieva, A. A. Firsov, *Science*, **2004**, *306*, 666.

[2] P. T. Yin, S. Shah, M. Chhowalla, K. Lee, Design, *Chem. Rev.*, **2015**, *115*, 2483.

[3] A. K. Geim, K. S. Novoselov, *Nat. Mater.*, **2007**, *6*, 183.

[4] M. D. Stoller, S. J. Park, Y. W. Zhu, J. H. An, R. S. Ruoff, *Nano Lett.*, **2008**, *8*, 3498.

[5] F. Bonaccorso, L. Colombo, G. Yu, M. Stoller, V. Tozzini, A. C. Ferrari, R. S. Ruoff, Vittorio Pellegrini, *Science*, **2015**, *347*, 1246501.

[6] A. Gulzar, P. Yang, F. He, J. Xu, D. Yang, L. Xu, M. O. Jan, *Chem. Biol. Interact.*, **2017**, *262*, 69.

[7] J. Ouyang, S. Rao, R. Liu, L. Wang, W. Chen, W. Tao, N. Kong, *Adv. Drug Deliv. Rev.*, **2022**, *185*, 114268.

[8] C. X. Hu, Y. Shin, O. Read, C. Casiraghi, *Nanoscale*, **2021**, *13*, 460.

[9] J. Liu, L. Cui, D. Losic, *Acta Biomater.*, **2013**, *9*, 9243.

[10] Y. Chen, Y. Su, S. Hu, S. Chen, *Adv. Drug Deliv. Rev.*, **2016**, *105*, 190.

[11] M. Liu, H. Zhu and Y. Wang, C. Sevencan, B. L. Li, *ACS Mater. Lett.*, **2021**, *3*, 462.

[12] D. Ma, C. Xie, T. Wang, L. Mei, X. Zhang, Z. Guo, W. Yin, *Chembiochem*, **2020**, *21*, 2373.

[13] S. S. Y. Chan, Y. S. Tan, K. X. Wu, C. Cheung, D. K. Loke, *ACS Appl. Bio. Mater.*, **2018**, *1*, 210.

[14] S. Anju, J. Ashtami, P.V. Mohanan, *Mater. Sci. Eng. C*, **2019**, *97*, 978.

[15] A. Ruiz, C. Martín, G. Reina, *Nanoscale Adv.*, **2021**, *3*, 4029.

[16] Z. Li, L. Zhu, Z. Cai, L. Chen, H. Zhu, *J. Phys. Mater.*, **2021**, *4*, 042004.

[17] M. Luo, T. Fan, Y. Zhou, H. Zhang, L. Mei, *Adv. Funct. Mater.*, **2019**, *29*, 1808306.

[18] N. Kong, X. Ji, J. Wang, X. Sun, G. Chen, T. Fan, W. Liang, H. Zhang, A. Xie, O. C. Farokhzad, W. Tao, *Nano Lett.*, **2020**, *20*, 3943.

[19] A. Merlo, V. R. S. S. Mokkapati, S. Pandit, I. Mijakovic, *Biomater. Sci.*, **2018**, *6*, 2298.

[20] B. Deng, Z. Liu, H. Peng, *Adv. Mater.*, **2018**, *31*, Toward Mass Production of CVD Graphene Films.

[21] D. Parviz, F. Irin, S. A. Shah, S. Das, C. B. Sweeney, M. J. Green, *Adv. Mater.*, **2016**, *28*, 8796.

[22] Y. Xu, H. Cao, Y. Xue, B. Li, W. Cai, *Nanomaterials*, **2018**, *8*, 942.

[23] K. Lobo, P. Sahoo, R. Kurapati, K. V. Krishna, V. Patil, A. Pandit, H. Matte, *Chem. Eur. J.*, **2021**, *27*, 7434.

[24] F. Lebre, D. Hanlon, J. B. Boland, J. Coleman, E. C. Lavelle, *Adv. Biosyst.*, **2018**, *2*, 1800102.

[25] W. Y. Yin, L. Yan, J. Yu, G. Tian, L. J. Zhou, X. P. Zheng, X. Zhang, Y. Yong, J. Li, Z. J. Gu, Y. L. Zhao, *ACS Nano*, **2014**, *8*, 6922.

[26] J. N. Coleman, M. Lotya, A. O'Neill, S. D. Bergin, P. J. King, U. Khan, K. Young, A. Gaucher, S. De, R. J. Smith, I. V. Shvets, S. K. Arora, G. Stanton, H. Y. Kim, K. Lee, G. T. Kim, G. S. Duesberg, T. Hallam, J. J. Boland, J. J. Wang, J. F. Donegan, J. C. Grunlan, G. Moriarty, A. Shmeliov, R. J. Nicholls, J. M. Perkins, E. M. Grieveson, K. Theuwissen, D. W. McComb, P. D. Nellist, V. Nicolosi, *Science*, **2011**, *331*, 568.

[27] E. P. Nguyen, B. J. Carey, T. Daeneke, J. Z. Ou, K. Latham, S. Zhuiykov, K. Kalantar-zadeh, *Chem. Mater.*, **2015**, *27*, 53.

[28] L. Chen, M. Qian, H. Jiang, Y. Zhou, Y. Du, Y. Yang, T. Huo, R. Huang, Y. Wang, *Biomaterials*, **2020**, *236*, 119770.

[29] S. J. Goldie, M. T. Degiacomi, S. Jiang, S. J. Clark, V. Erastova, K. S. Coleman, *ACS Nano*, **2022**, *16*, 16109.

[30] A. Jawaid, D. Nepal, K. Park, M. Jespersen, A. Qualley, P. Mirau, L. F. Drummy, R. A. Vaia, *Chem. Mater.*, **2016**, *28*, 337.

[31] C. Xing, S. Chen, M. Qiu, X. Liang, Q. Liu, Q. Zou, Z.n Li, Z. Xie, D. Wang, B. Dong, L. Liu, D. Fan, H. Zhang, *Adv. Healthcare Mater.*, **2018**, *7*, 1701510.

[32] Y. Li, Z. Du, X. Liu, M. Ma, D. Yu, Y. Lu, J. Ren, X. Qu, *Small*, **2019**, *15*, e1901116.

[33] S. Wan, B. Zhang, S. Li, B. He, Y. Pu, *J. Mater. Chem. B*, **2020**, *8*, 2805.

[34] C. K. Su, H. Q. Zhong, H. L. Chen, Y. X. Guo, Z. Y. Guo, D. Q. Huang, W. Zhang, Q. Wu, B. W. Yang, Z. M. Liu, *New J. Chem.*, **2019**, *43*, 8620.

[35] H. Wang, L. Zhong, Y. Liu, X. Xu, C. Xing, M. Wang, S. M. Bai, C. H. Lu, H. H. Yang, *Chem. Commun.*, **2018**, *54*, 3142.

[36] H. L. Zheng, B. X. Ma, Y. S. Shi, Q. X. Dai, D. S. Li, E. Ren, J. Zhu, J. M. Liu, H. Chen, Z. Y. Yin, C. C. Chu, X. M. Wang, G. Liu, *Chem. Eng. J.*, **2021**, *406*, 126888.

[37] H. Yi, X. Zhou, C. Zhou, Q. Yang, N. Jia, *Biomater. Sci.*, **2021**, *9*, 148.

[38] P. Shah, T. N. Narayanan, C. Z. Li, S. Alwarappan, *Nanotechnology*, **2015**, *26*, 315102.

[39] H. Fu, Z. Li, H. Xie, Z. Sun, B. Wang, H. Huang, G. Han, H. Wang, P. K. Chu, X. F. Yu, *RSC Adv.*, **2017**, *7*, 14618.

[40] R. Kurapati, L. Muzi, A. Garibay, J. Russier, D. Voiry, I. A. Vacchi, M. Chhowalla, A. Bianco, *Adv. Funct. Mater.*, **2017**, *27*, 1605.

[41] R. Kurapati, C. Backes, C. Ménard-Moyon, J. N. Coleman, A. Bianco, *Angew. Chem.*, **2016**, *128*, 5596.

[42] C. Backes, N. C. Berner, X. Chen, P. Lafargue, P. LaPlace, M. Freeley, G. S. Duesberg, J. N. Coleman, A. R. McDonald, *Angew. Chem. Int. Ed.*, **2015**, *54*, 2638.

[43] Y. Wang, J. Xie, J. Kang, W. Choi, P. Jangili, B. Zhang, N. Xie, G. Nie, J. He, H. Zhang, L. Liu, J. S. Kim, *Adv. Funct. Mater.*, **2020**, *30*, 2003338.

[44] Wang, C. C. Ge, W. Y. Liang, Q. H. Yang, Q. Liu, W. Ma, L. L. Shi, H. Wu, Y. H. Zhang, Z. Z. Wu, C. Y. Wei, L. D. Huang, Z. Y. Fang, L. P. Liu, S. Y. Bao, H. Zhang, *Adv. Sci.*, **2020**, *7*, 2000940.

[45] Z. Sun, Y. Zhang, H. Yu, C. Yan, Y. Liu, S. Hong, H. Tao, A. W. Robertson, Z. Wang, A. A. H. Padua, *Nanoscale*, **2018**, *10*, 12543.

[46] S. P. Ogilvie, M. J. Large, M. A. O'Mara, P. J., Lynch, C. L., Lee, A. A. K. King, A. C. Backes, A. B. Dalton, *2D Mater.*, **2019**, *6*, 031002.

[47] S. J. Goldie, M. T. Degiacomi, S. Jiang, S. J. Clark, V. Erastova, K. S. Coleman, *ACS Nano*, **2022**, *16*, 16109.

[48] R. W. Harries, C. J. Brown, L. Woodbine, A. Amorim Graf, M. J. Large, K. Clifford, P. J. Lynch, S. P. Ogilvie, A. B. Dalton, A. A. K. King, *ACS Appl. Nano Mater.*, **2021**, *4*, 2002.

[49] M. Yi, Z. G. Shen, S. S. Liang, L. Liu, X. J. Zhang, S. L. Ma, *Chem. Commun.*, **2013**, *49*, 11059.

[50] X. K. Cai, Y. T. Luo, B. Liu, H. M. Cheng, *Chem. Soc. Rev.*, **2018**, *47*, 6224.

[51] S. S. Y. Chan, D. Lee, M. P. Meivita, L. Li, Y. S. Tan, N. Bajalovic, D. K. Loke, *Nanoscale Adv.*, **2021**, *3*, 6974.

[52] D. Lee, S. S. Y. Chan, J. S. Naikar, M. P. Meivita, W. C. Teoh, N. Bajalovic, D. K. Loke, *Mater. Adv.*, **2023**, *4*, 291.

[53] H. Wang, X. Yang, W. Shao, S. Chen, J. Xie, X. Zhang, J. Wang, Y. Xie, *J. Am. Chem. Soc.*, **2015**, *137*, 11376.

[54] X. Zhang, Z. Zhang, S. Zhang, D. Li, W. Ma, C. Ma, F. Wu, Q. Zhao, Q. Yan, B. Xing, *Small*, **2017**, *13*, 1701210.

[55] W. Tao, X. Zhu, X. Yu, X. Zeng, Q. Xiao, X. Zhang, X. Ji, X. Wang, J. Shi, H. Zhang, L. Mei, *Adv. Mater.*, **2017**, *29*, 1603276.

[56] D. Yang, G. Yang, P. Yang, R. Lv, S. Gai, C. Li, F. He, J. Lin, *Adv. Funct. Mater.*, **2017**, *27*, 1700371.

[57] J. Kim, S. Kwon, D. H. Cho, B. Kang, H. Kwon, Y. Kim, S. O. Park, G. Y. Jung, E. Shin, W. G. Kim, H. Lee, G. H. Ryu, M. Choi, T. H. Kim, J. Oh, S. Park, S. K. Kwak, S. W. Yoon, D. Byun, Z. Lee, C. Lee, *Nat. Commun.*, **2015**, *6*, 8294.

[58] K. B. Ricardo, A. Sendecki, H. Liu, *Chem. Commun.*, **2014**, *50*, 2751.

[59] A. Kalosi, M. Labudova, A. Annusova, M. Benkovicova, M. Bodik, J. Kollar, M. Kotlar, P. Kasak, M. Jergel, S. Pastorekova, P. Siffalovic, E. Majkova, *Biomater. Sci.*, **2020**, *8*, 1973.

[60] M. Bae, J. K. Oh, S. Liu, N. Nagabandi, Y. Yegin, W. DeFlorio, L. Cisneros-Zevallos, E. M. A. Scholar, *Nanomaterials*, **2021**, *11*, 1453.

[61] J. Kaur, M. Singh, C. Dell'Aversana, R. Benedetti, P. Giardina, M. Rossi, M. Valadan, A. Vergara, A. Cutarelli, A. M. I. Montone, L. Altucci, F. Corrado, A. Nebbioso, C. Altucci, *Sci. Rep.*, **2018**, *8*, 16386.

[62] L. Q. Mei, X. Zhang, W. Y. Yin, X. H. Dong, Z. Guo, W. H. Fu, C. J. Su, Z. J. Gu, Y. L. Zhao, *Nanoscale*, **2019**, *11*, 4767.

[63] K. G. Zhou, N. N. Mao, H. X. Wang, Y. Peng, H. L. Zhang, *Angew. Chem. Int. Ed.*, **2011**, *50*, 10839.

[64] L. Jia, L. Ding, J. Tian, L. Bao, Y. Hu, H. Ju, J. S. Yu, *Nanoscale*, **2015**, *7*, 15953.

[65] P. Štefík, A. Annušová, B. Lakatoš, K. Elefantová, L. Čepcová, M. Hofbauerová, A. Kálosi, M.j Jergel, E. Majková, P. Šiffalovič, *Biomed. Mater.*, **2021**, *16*, 055009.

[66] Y. Lin, D. Han, Y. Li, L. Tan, X. Liu, Z. Cui, X. Yang, Z. Li, Y. Liang, S. Zhu, S. Wu, *ACS Sustain. Chem. Eng.*, **2019**, *7*, 14982.

[67] M. G. Raucci, I. Fasolino, M. Caporali, M. Serrano-Ruiz, A. Soriente, M. Peruzzini, L. Ambrosio, *ACS Appl. Mater. Interfaces*, **2019**, *11*, 9333.

[68] D. Parviz, S. Das, H. S. T. Ahmed, F. Irin, S. Bhattacharia, M. J. Green, *ACS Nano*, **2012**, *6*, 8857.

[69] D. McManus, S. Vranic, F. Withers, V. Sanchez-Romaguera, M. Macucci, H. Yang, R. Sorrentino, K. Parvez, S. K. Son, G. Iannaccone, K. Kostarelos, G. Fiori, C. Casiraghi, *Nat. Nanotechnol.*, **2017**, *12*, 343.

[70] G. Peng, S. Keshavan, L. Delogu, Y. Shin, C. Casiraghi, B. Fadeel, *Small*, **2022**, *18*, e2107816.

[71] Y. Shin, S. Vranic, X. Just-Baringo, S. M. Gali, T. Kisby, Y. Chen, A. Gkoutzidou, E. Prestat, D. Beljonne, I. Larrosa, K. Kostarelos, C. Casiraghi, *Nanoscale*, **2020**, *12*, 12383.

[72] C. X. Hu, O. Read, Y. Shin, Y. Chen, J. Wang, M. Boyes, N. Zeng, A. Panigrahi, K. Kostarelos, I. Larrosa, S. Vranic, C. Casiraghi, *ACS Appl. Nano Mater.*, **2022**, *5*, 12626.

[73] V. T. H. Pham, V. K. Truong, M. D. J. Quinn, S. M. Notley, Y. C. Guo, V. A. Baulin, M. Al Kobaisi, R. J. Crawford, E. P. Ivanova, *ACS Nano*, **2015**, *9*, 8458.

[74] S. Doktorovova, E. B. Souto, A. M. Silva, *Eur. J. Pharm. Biopharm.*, **2014**, *87*, 1.

[75] M. D. J. Quinn, T. Wang, S. M. Notley, Surfactant-exfoliated graphene as a near-infrared photothermal ablation agent, *Biomed. Phys. Eng. Express.*, **2018**, *4*, 025020.

[76] M. Llenas, L. Cuenca, C. Santos, I. Bdikin, G. Goncalves, G. Tobias-Rossell, *Biomedicines*, **2022**, *10*, 3238.

[77] D. Jana, S. Jia, A. K. Bindra, P. Xing, D. Ding, Y. Zhao, *ACS Appl. Mater. Interfaces*, **2020**, *12*, 18342.

[78] H. Lee, M. Koo, C. Park, M. Patel, H. Han, T. H. Park, P. Kumar, W. G. Koh, C. Park, *Nano Research*, **2020**, *13*, 2726.

[79] A. B. Bourlinos, V. Georgakilas, R. Zboril, T. A. Steriotis, A. K. Stubos, C. Trapalis, *Solid State Commun.*, **2009**, *149*, 2172.

[80] Z. M. Markovic, L. M. Harhaji-Trajkovic, B. M. Todorovic-Markovic, D. P. Kepic, K. M. Arsikin, S. P. Jovanovic, A. C. Pantovic, M. D. Dramicanin, V. S. Trajkovic, *Biomaterial*s, **2011**, *32*, 1121.

[81] N. Wang, F. Wei, Y. Qi, H. Li, X. Lu, G. Zhao, Q. Xu, *ACS Appl. Mater. Interfaces*, **2014**, *6*, 19888.

[82] J. Cui, Z. Song, L. Xin, S. Zhao, Y. Yan, G. Liu, *Carbon*, **2016**, *99*, 249.

[83] F. Bani, A. Bodaghi, A. Dadkhah, S. Movahedi, N. Bodaghabadi, M. Sadeghizadeh, M. Adeli, *Lasers Med. Sci.*, **2018**, *33*, 795.

[84] S. Ganguly, D. Ray, P. Das, P. P. Maity, S. Mondal, V. K. Aswal, S. Dhara, N. C. Das, *Ultrason. Sonochem.*, **2018**, *42*, 212.

[85] G. Guan, S. Zhang, S. Liu, Y. Cai, M. Low, C. P. Teng, I. Y. Phang, Y. Cheng, K. L. Duei, B. M. Srinivasan, Y. Zheng, Y. W. Zhang, M. Y. Han, *J. Am. Chem. Soc.*, **2015**, *137*, 6152.

[86] J. Wang, Y. Li, G. Nie, *Nat. Rev. Mater.*, **2021**, *6*, 766.

[87] A. D. Parab, R. Dureja, R. Rao, J. M. Slocik, R. R. Naik, T. R. Walsh, M. R. Knecht, *Langmuir*, **2021**, *37*, 1152.

[88] S. N. Kim, Z. Kuang, J. M. Slocik, S. E. Jones, Y. Cui, B. L. Farmer, M. C. McAlpine, R. R. Naik, *J. Am. Chem. Soc.*, **2011**, *133*, 14480.

[89] M. Cao, N. Wang, L. Wang, Y. Zhang, Y. Chen, Z. Xie, Z. Li, E. Pambou, R. Li, C. Chen, F. Pan, H. Xu, J. Penny, J. R. P. Webster, J. R. Lu, *J. Mater. Chem. B*, **2016**, *4*, 152.

[90] A. D. Parab, A. Budi, J. M. Slocik, R. Rao, R. R. Naik, T. R. Walsh, M. R. Knecht, *J. Phys. Chem. C*, **2020**, *124*, 2219.

[91] L. Zhang, Y. B. Sheng, A. Z. Yazdi, K. Sarikhani, F. Wang, Y. S. Jiang, J. W. Liu, T. Zheng, W. Wang, P. K. Ouyang, P. Chen, *Nanoscale*, **2019**, *11*, 2999.

[92] B. Ojha, G. Das, *J. Phys. Chem. B*, **2010**, *114*, 3979.

[93] K. L. Zhou, D. Q. Pan, Y. Y. Lou, J. H. Shi, *J. Mol. Recognit.*, **2018**, *31*, e2716.

[94] R. Deng, H. Yi, F. Fan, L. Fu, Y. Zeng, Y. Wang, Y. Li, Y. Liu, S. Ji, Y. Su, *RSC Adv.*, **2016**, *6*, 77083.

[95] D. G. Thomas, S. De-Alwis, S. Gupta, V. K. Pecharsky, D. Mendivelso-Perez, R. Montazami, E. A. Smith, N. N. Hashemi, *R. Soc. Open Sci.*, **2021**, *8*, 200911.

[96] D. Alberghina, C. Giannetto, I. Vazzana, V. Ferrantelli, Giuseppe Piccione, *J. Vet. Diagn. Investig.*, **2011**, *23*, 111.

[97] A. Pattammattel, P. Pande, D. Kuttappan, M. Puglia, A. K. Basu, M. A. Amalaradjou, C. V. Kumar, *Langmuir*, **2017**, *33*, 14184.

[98] A. Vasconcelos, G. Freddi, A. Cavaco-Paulo, *Biomacromolecules*, **2008**, *9*, 1299.

[99] X. Zhang, L. Wang, Q. Lu, D. L. Kaplan, *ACS Appl. Mater. Interfaces*, **2018**, *10*, 22924.

[100] H. Zhuo, X. Zhang, L. Wang, Q. Lu, D. L. Kaplan, *ACS Sustain. Chem. Eng.*, **2018**, *6*, 12261.

[101] X. W. Huang, J. J. Wei, T. Liu, X. L. Zhang, S. M. Bai, H. H. Yang, *Nanoscale*, **2017**, *9*, 17193.

[102] D. Joseph, N. Tyagi, A. Ghimire, K. E. Geckeler, *RSC Adv.*, **2014**, *4*, 4085.

[103] Siepi, E. Morales-Narváez, N. Domingo, D.M. Monti, E. Notomista, A. Merkoçi, *2D Mater.*, **2017**, *4*, 035007.

[104] X. Xu, J. Wu, Z. Meng, Y. Li, Q. Huang, Y. Qi, Y. Liu, D. Zhan, X. Y. Liu, *ACS Appl. Nano Mater.*, **2018**, *1*, 5460.

[105] J. W. Hu, J. R. Hou, S. S. Huang, L. Zong, X. D. Li, Z. J. Zhang, Y. X. Duan, J. M. Zhang, *Carbon*, **2020**, *157*, 448.

[106] Ge, J. L. Wang, Z. X. Shi, J. Yin, *J. Mater. Chem.*, **2012**, *22*, 17619.

[107] P. Tiwari, N. Kaur, V. Sharma, S. M. Mobin, *Phys. Chem. Chem. Phys.*, **2018**, *20*, 20096.

[108] M. Cosgrove, Nucleotides, *Nutrition*, **1998**, *14*, 748.

[109] M. Ayan-Varela, J. I. Paredes, L. Guardia, S. Villar-Rodil, J. M. Munuera, M. Diaz-Gonzalez, C. Fernandez-Sanchez, A. Martinez-Alonso, J. M. Tascon, *ACS Appl. Mater. Interfaces*, **2015**, *7*, 10293.

[110] M. Cicuendez, M. Fernandes, M. Ayan-Varela, H. Oliveira, M. J. Feito, R. Diez-Orejas, J. I. Paredes, S. Villar-Rodil, M. Vila, M. T. Portoles, I. F. Duarte, *Colloids Surf. B*, **2020**, *186*, 110709.

[111] M. Cicuendez, A. Coimbra, J. Santos, H. Oliveira, M. Ayan Varela, J. I. Paredes, S. Villar Rodil, M. Vila, V. S. Silva, *ACS Appl. Bio. Mater.*, **2021**, *4*, 4384.

[112] A. Ruiz, M. A. Lucherelli, D. Murera, D. Lamon, C. Ménard-Moyon, A. Bianco, *Carbon*, **2020**, *170*, 347.

[113] M. Ayan-Varela, O. Perez-Vidal, J. I. Paredes, J. M. Munuera, S. Villar-Rodil, M. Diaz-Gonzalez, C. Fernandez-Sanchez, V. S. Silva, M. Cicuendez, M. Vila, A. Martinez-Alonso, J. M. Tascon, *ACS Appl. Mater. Interfaces*, **2017**, *9*, 2835.

[114] B. Caridad, J. I. Paredes, O. Pérez–Vidal, S. Villar–Rodil, A. Pagán, J. L. Cenis, A. Martínez-Alonso, J. M. D. Tascón, *Carbon*, **2018**, *129*, 321.

[115] M. Cicuendez, V. S. Silva, J. Santos, A. Coimbra, H. Oliveira, M. Ayan-Varela, J. I. Paredes, S. Villar-Rodil, M. Vila, *Mater. Sci. Eng. C*, **2019**, *100*, 11.

[116] G. S. Bang, S. Cho, N. Son, G. W. Shim, B. K. Cho, S. Y. Choi, *ACS Appl. Mater. Interfaces*, **2016**, *8*, 1943.

[117] Z. Miao, D. Huang, Y. Wang, W. J. Li, L. Fan, J. Wang, Y. Ma, Q. Zhao, Z. Zha, *Adv. Funct. Mater.*, **2020**, *30*, 2001593.

[118] K. R. Paton, E. Varrla, C. Backes, R. J. Smith, U. Khan, A. O'Neill, C. Boland, M. Lotya, O. M. Istrate, P. King, T. Higgins, S. Barwich, P. May, P. Puczkarski, I. Ahmed, M. Moebius, H. Pettersson, E. Long, J. Coelho, S. E. O'Brien, E. K. McGuire, B. M. Sanchez, G. S. Duesberg, N. McEvoy, T. J. Pennycook, C. Downing, A. Crossley, V. Nicolosi, J. N. Coleman, *Nat. Mater.*, **2014**, *13*, 624.

[119] M. Lotya, P. J. King, U. Khan, S. De, J. N. Coleman, *ACS Nano*, **2010**, *4*, 3155.

[120] L. Di Cristo, S. Mc Carthy, K. Paton, D. Movia, A. Prina-Mello, *2D Mater.*, **2018**, *5*, 045033.

[121] J. McIntyre, N. K. Verma, R. J. Smith, C. Moore, H. Nerl, N. McEvoy, N. Berner, I. McGovern, U. Khan, P. Lyons, L. O'Neill, V. Nicolosi, G. S. Duesberg, H. J. Byrne, J. Coleman, Y. Volkov, *RSC Adv.*, **2016**, *6*, 65299.

[122] R. J. Smith, P. J. King, M. Lotya, C. Wirtz, U. Khan, S. De, A. O'Neill, G. S. Duesberg, J. C. Grunlan, G. Moriarty, J. Chen, J. Wang, A. I. Minett, V. Nicolosi, J. N. Coleman, *Adv. Mater.*, **2011**, *23*, 3944.

[123] X. Liu, G. Duan, W. Li, Z. Zhou, R. Zhou, *RSC Adv.*, **2017**, *7*, 37873.

[124] C. Moore, D. Movia, R. J. Smith, D. Hanlon, F. Lebre, E. C. Lavelle, H. J. Byrne, J. N. Coleman, Y. Volkov, J. McIntyre, *2D Mater.*, **2017**, *4*, 025065.

[125] N. O. Peña, K. Cherukula, B. Even, D. Ji, S. Razafindrakoto, S. Peng, A. K. A. Silva, C. Ménard-Moyon, H. Hillaireau, A. Bianco, E. Fattal, D. Alloyeau, F. Gazeau, *Adv. Mater.*, **2023**, *35*, 2209615.

[126] M. A. Lucherelli, X. L. Qian, P. Weston, M. Eredia, W. P. Zhu, P. Samori, H. J. Gao, A. Bianco, A. V. Bussche, *Adv. Mater.*, **2021**, *33*, 2103137.

[127] V. J. González, A. M. Rodríguez, V. León, J. Frontiñán-Rubio, J. L. G. Fierro, M. Durán-Prado, A. B. Muñoz-García, M. Pavone, E. Vázquez, *Green Chem.*, **2018**, *20*, 3581.

[128] S. S. Xing, C. Q. Xia, X. Y. Liu, L. Q. Guo, F. F. Fu, *Mater. Adv.*, **2022**, *3*, 3593.

[129] Y. Zhang, T. Sun, C. Jiang, *Acta. Pharm. Sin. B*, **2018**, *8*, 34.

[130] J. M. Malho, P. Laaksonen, A. Walther, O. Ikkala, M. B. Linder, *Biomacromolecules*, **2012**, *13*, 1093.

[131] F. Zhang, X. J. Chen, R. A. Boulos, F. M. Yasin, H. B. Lu, C. Raston, H. B. Zhang, *Chem. Commun.*, **2013**, *49*, 4845.

[132] S. Roy, A. Mondal, V. Yadav, A. Sarkar, R. Banerjee, P. Sanpui, A. Jaiswal, *ACS Appl. Bio. Mater.*, **2019**, *2*, 2738.

[133] R. Zou, S. Shan, L. Huang, Z. Chen, T. Lawson, M. Lin, L. Yan, Y. Liu, *ACS Biomater. Sci. Eng.*, **2020**, *6*, 673-679.

Biographies

Yilin He obtained her Master in material engineering in 2020 under the supervision of Dr. Renjun Pei at the Institute of Nano-Tech and Nano-Bionics, Chinese Academy of Sciences in Suzhou. She is currently a PhD student under the co-supervision of Dr. Alberto Bianco and Dr. Cécilia Ménard-Moyon at the Institute of Cellular and Molecular Biology (CNRS, Strasbourg). Her research interests focus mainly in the design and synthesis of nanomaterials for combined cancer therapy.

Andrés Felipe Andrade obtained his Master in 2021 in supramolecular chemistry from the CSC Graduate School of the University of Strasbourg under the supervision of Dr. Alberto Bianco. His research interests focus mainly in exploring chemical strategies to exfoliate and functionalize different types of two-dimensional materials.

Dr. Cécilia Ménard-Moyon is CNRS Researcher since 2008 in the Laboratory of Immunology, Immunopathology and Therapeutic Chemistry in Strasbourg (France). Her research interests are focused on the functionalization of different types of nanoparticles and carbon-based nanomaterials for biomedical applications, self-assembly of amino acid derivatives and peptides, and formation of hydrogels for on-demand drug delivery. She has published 105 articles and 10 book chapters. She is the coordinator of the Horizon Europe Marie Skłodowska-Curie Actions Doctoral Networks “Melomanes” project (2023-27) on the synthesis of

multifunctional magnetic nanoparticles for combination therapy to treat metastatic melanoma (https://melomanes.eu/).

Dr. Alberto Bianco received his PhD in 1996 from the University of Padova. As a visiting scientist, he worked at the University of Lausanne, the University of Tübingen (as an Alexander von Humboldt fellow), the University of Padova and Kyoto University. He is currently Research Director at the CNRS in Strasbourg. His research interests focus on the design of multifunctional carbon-based and 2D materials for therapy, diagnostics and imaging. He is Fellow of the European Academy of Science and Academia Europaea, and in 2019 he has obtained the CNRS Silver Medal. Since 2011 he is Editor of the journal CARBON.

Two-dimensional (2D) materials can be effectively produced by liquid phase exfoliation (LPE). using different conditions. LPE generated 2D materials in aqueous solutions, represented by graphene, black phosphorus, transition metal dichalcogenides and hexagonal boron nitride, possess a huge potential in the biomedical domains, spanning cancer therapy, drug delivery as well as antimicrobial and biosensing.

Y. He, A. F. Andrade, C. Ménard-Moyon,* A. Bianco*

Biocompatible 2D Materials via Liquid Phase Exfoliation